

**Ruthenium (II) polypyridyl complexes as
photoprobes for DNA mismatches**

by

Paul Tiley

**A thesis submitted to Swansea University in fulfilment of the requirements
for the degree of Master of Science in Chemistry by Research**

Department of Chemistry

Swansea University

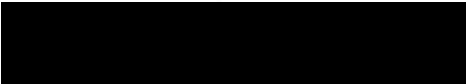
January 2022

Abstract

[Ru(bpy)₂dppz]²⁺ is a classic “light switch” effect complex with a brighter emission for mismatched DNA than well-matched DNA. It is, therefore, a photoprobe for DNA. To enhance its selectivity for mismatched base pairs which can lead to DNA mutations, a range of related complexes were synthesized and investigated. The approach involved increasing the steric bulk of the ancillary 2,2'-bipyridine (bpy) ligands and/or the dipyridophenazine (dppz) functional group ligand. This functional group ligand is known to insert or intercalate between adjacent base pairs in the base stack of DNA and an alternative functional group ligand was also explored: 12,17-dihydronaphthodipyridophenazine-12,17-dione (aqphen). Hairpin and 12 base oligonucleotide duplex DNA containing mismatched base pairs were tested and compared to the same sequences containing well-matched base pairs. Methylation of the ancillary bpy ligands only at positions 5,5' with dppz as the functional group ligand is highly selective for both the CC and the TT mismatches. For the former the signal is between 4 and 6.3x higher than it is for well-matched DNA and for the latter a 6x increase was recorded. It almost certainly binds to the DNA via intercalation and its performance in these experiments have identified a useful photoprobe for the identification of these mismatched base pairings. Methylation of the dppz functional group ligand at positions 10 and 12 produced large increases in emission intensity compared to the parent compound [Ru(bpy)₂dppz]²⁺ but did not substantially increase the mismatch base pair selectivity. The use of aqphen instead of dppz as the functional group ligand increased the binding strength with DNA and, notably, it showed a higher binding affinity for a 12mer duplex containing a CC mismatched base pair versus the well-matched sequence; its mode of binding is likely to be intercalation. In summary, enhancing steric bulk through methylation of the ancillary bpy ligands has achieved the desired selectivity whilst the same modification to the inserting dppz functional group ligand has led to large increases in signal intensity without an improvement in selectivity. The use of aqphen as the functional group ligand, which also has a greater steric bulk compared to dppz, increased binding affinity as well as selectivity.

Declarations

This work has not previously been accepted in substance for any degree and is not being concurrently submitted in candidature for any degree.

Signed..... 

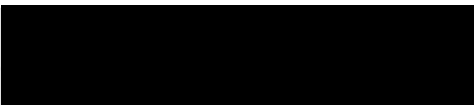
Date.....19th January 2022.....

This thesis is the result of my own investigations, except where otherwise stated. A bibliography is appended.

Signed..... 

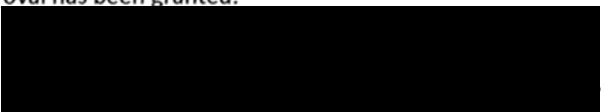
Date..... 19th January 2022.....

I hereby give consent for my thesis, if accepted, to be available for photocopying and for inter-library loan, and for the title and summary to be made available to outside organisations.

Signed..... 

Date..... 19th January 2022.....

The University's ethical procedures have been followed and, where appropriate, that ethical approval has been granted.

Signed..... 

Date..... 19th January 2022.....

Acknowledgements

My sincere thanks go to Dr Martin Gill, my supervisor, for all his support, patience, advice and encouragement throughout both the experimental and the written phases of my research.

Grateful thanks also go to Dr Chris Elgar, Postdoctoral Researcher, for the expert guidance provided from start to finish.

I could not have done this without them!

Contents

	Page
Abstract	2
Declarations	3
Acknowledgements	4
Contents	5
1. Introduction	6
• 1.1 Structure of DNA	6
• 1.2 Photoprobes	6
• 1.3 Luminescence	8
• 1.4 The "light switch" effect	9
• 1.5 DNA and the "light switch" effect	12
• 1.6 Aim of study	13
2. Experimental Procedures	15
• 2.1 Preparation of complexes	15
• 2.2 Photophysical characterization	30
• 2.3 DNA binding studies	32
3. Results and Discussion	36
• 3.1 Syntheses	36
• 3.2 UV/VIS absorption spectra	39
• 3.3 Luminescence excitation and emission spectra	40
• 3.4 Luminescence Quantum Yields Q at $\lambda_{\text{ex}} = 450\text{nm}$	44
• 3.5 DNA binding studies	45
○ 3.5.1 CT DNA	45
○ 3.5.2 Hairpin DNA	52
○ 3.5.3 12 base oligonucleotide duplex DNA (12mers)	58
4. Conclusions	64
References	68

1. Introduction

1.1 Structure of DNA

Watson-Crick base pairs are the building blocks of the DNA double-helix. The sugar-phosphate backbone in each strand is held together by hydrogen bonds between the nucleotides which form each base pair. This allows the DNA duplex to maintain a regular helical structure, the specificity of which is determined by the precise sequence of base pairs. Failures in the mechanism through which DNA replicates can lead to the formation of non Watson-Crick or mismatch base pairs. DNA has its own mismatch repair (MMR) machinery to prevent such errors but cells deficient in MMR proteins cannot correct mismatches generated by these errors. These can, in turn, lead to mutations which can be the starting point for the development of diseases such as cancer. For example, 10.1% of endometriosis-associated ovarian carcinomas showed a loss of MMR protein expression as well as up to 51% of colorectal cancers in patients < 60 years of age exhibited a complete loss of combinations of the four major MMR proteins.^{1,2}

1.2 Photoprobes

The development of small molecules which specifically target duplex DNA base pair mismatches is an area of great interest and potential in terms of both detecting and treating the cancer at the earliest possible stages.³ In particular, the use of transition metal complexes as a new type of DNA photoprobe has been of great interest since the 1990s given the flexibility of their structures which can incorporate a wide variety of co-ordinated organic ligands, as well as their inherent photophysical properties.⁴ Specifically for mismatch-targeting, Pierard and Kirsch-De Mesmaeker investigated rhenium, ruthenium and rhodium complexes whilst the Barton group found that octahedral rhodium complexes with sterically expansive aromatic ligands bind to DNA mismatches with high affinity and selectivity via metalloinsertion, extruding the mismatches (**Fig. 1**):⁵⁻⁸

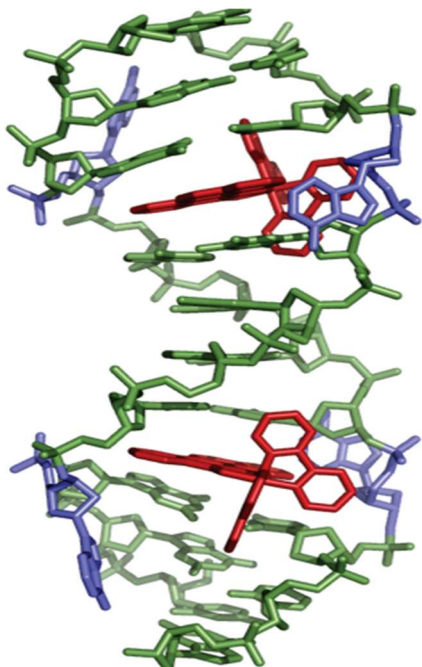


Fig. 1 Model of crystal structure of Δ -[Rh(bpy)₂(chrysi)]³⁺ inserted into the oligonucleotide 5'-CGGAAATTACCG-3' from data generated by X-ray crystallography. Two complex molecules are shown in red, one inserted into each AA mismatch of the oligonucleotide coloured green. The ejected adenosines are shown in blue.⁶

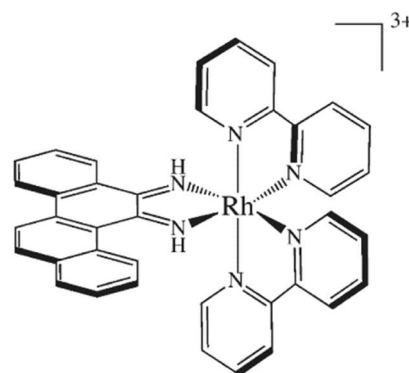


Fig. 2 Δ -[Rh(bpy)₂(chrysi)]³⁺ in which bpy = 2,2'-bipyridine and chrysi = 5,6-chrysenequinone diamine.

The drawback is that rhodium complexes are non-emissive.⁹ In parallel to this work, the Barton group has also developed ruthenium complexes that bind DNA structures, including mismatch-containing sequences.¹⁰⁻¹² These have the benefit that they are able to function as molecular “light switches” for DNA. This class of transition metal complex luminesces from an MLCT (metal-to-ligand charge-transfer) state in aprotic solvents whilst, in aqueous solution, their luminescence is quenched due to hydrogen bonding with water. Upon intercalation between the base pairs in the DNA double helix (the base stack), the hydrophobic environment acts like an aprotic solvent meaning that these complexes luminesce brightly as they are no longer quenched by water.^{12,13} This is typified by [Ru(bpy)₂dppz]²⁺, the first MLCT “light switch” for DNA (**Fig. 3**) and has seen a vast number of ruthenium polypyridyl complexes developed by the Barton group and others including Chao *et al.* for a variety of DNA binding properties.¹⁴⁻¹⁶ The modifications have involved making the ligands asymmetric, more polar using amine or ester groups or more hydrophobic by increasing the number of aromatic rings or using longer carbon chains.

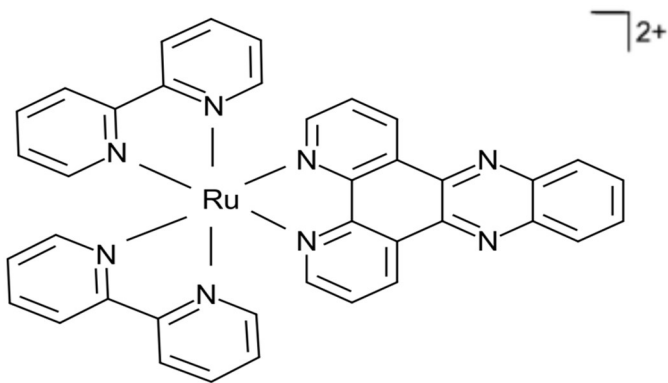


Fig. 3 Chemical structure of complex 1 $[\text{Ru}(\text{bpy})_2\text{dppz}]^{2+}$ in which bpy = 2,2'-bipyridine and dppz = dipyrrophenazine

1.3 Luminescence

Luminescence can be explained by the Jablonski diagram (**Fig. 4**).¹⁷

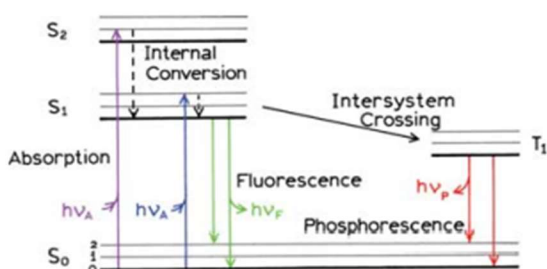


Fig. 4 Jablonski diagram: S_0 , S_1 and S_2 are the singlet ground, first and second electronic states respectively. 0, 1, 2, etc. are the different vibrational levels within each electronic energy level. T_1 is the first triplet excited state. $h\nu_A$ is the light energy absorbed when the electron is excited either to S_1 or to S_2 . $h\nu_F$ is the light energy emitted during fluorescence when the electron returns to S_0 from S_1 . $h\nu_P$ is the light energy emitted during phosphorescence when the electron returns to S_0 from T_1 .¹⁷

Once light is absorbed the molecule is usually excited from S_0 to a higher vibrational level of either S_1 or S_2 . Internal conversion takes place releasing non-radiative energy as the molecule normally relaxes to the lowest vibrational level of S_1 . Fluorescence can then occur emitting radiation as the molecule transitions back to S_0 and typically to an excited vibrational level of S_0 . Finally, further non-radiative emission takes place as the molecule relaxes to the lowest vibrational level of S_0 . The loss of non-radiative energy through vibrational relaxation explains why the wavelength of fluorescent light emitted is always longer or of a lower energy than that of the light absorbed. This is the Stokes Shift.¹⁸ Equally the tendency to relax to the lowest vibrational level is described by Kasha's rule: the emitting level of a given multiplicity is the lowest level of that multiplicity.¹⁹ In essence this means that fluorescence only occurs with an appreciable yield from the lowest excited state of a given multiplicity: the lowest vibrational level of S_1 in this case.

Intersystem crossing can also occur which means that the electron in the molecule in the S_1 state changes its direction of spin (spin conversion) and moves to the first triplet excited state T_1 . Radiative emission from T_1 or phosphorescence then returns the molecule to S_0 once more. Phosphorescence usually involves the emission of longer wavelengths of light than fluorescence and, because transitions from T_1 to S_0 are forbidden, it is slower (milliseconds or seconds as opposed to nanoseconds).¹⁷ The luminescence in ruthenium complexes is phosphorescence as it is due to transitions from T_1 to S_0 .

1.4 The “light switch” effect

To explain the “light switch” effect, complex 1 below can be considered (**Fig. 5**):

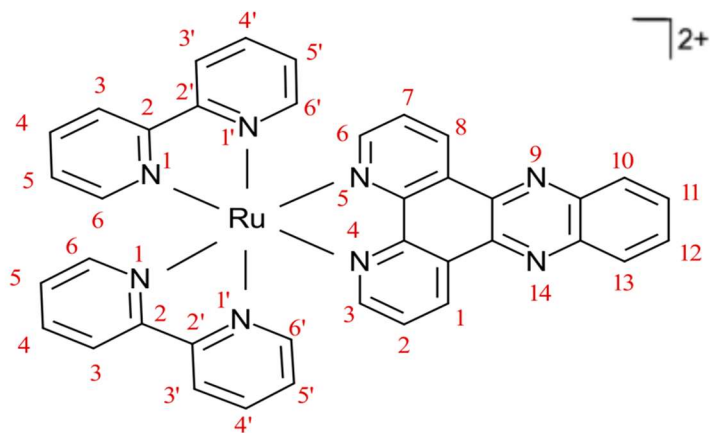
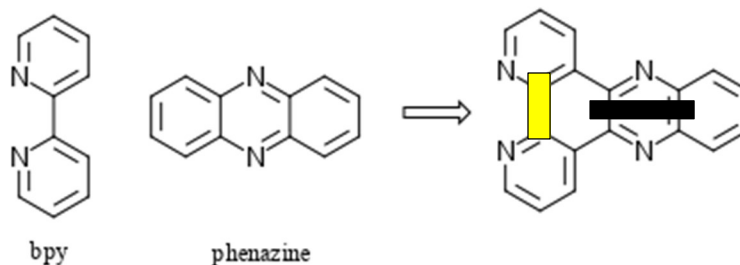


Fig. 5 Numbering of bpy and dppz in complex 1 $[\text{Ru}(\text{bpy})_2\text{dppz}]^{2+}$

This is a classic “light switch” effect complex.²⁰ The mechanism can be explained by the existence of two close-lying metal-to-ligand charge-transfer (MLCT) states on the dppz ligand: a bright primary state (MLCT') localized on the bpy component of the dppz ligand which luminesces and a dark secondary state (MLCT'') situated largely on the phenazine section of the ligand which is non-luminescent as proposed by Olson *et al.* (**Fig. 6**).²¹



Bright or primary MLCT' state =

Dark or secondary MLCT'' state =

Fig. 6 Bright primary MLCT' and dark secondary MLCT'' states on dppz ligand.

Based on this model, the bright state is lowest in energy for aprotic solvents which leads to an emissive excited state. In protic solvents such as water, hydrogen bonding with the phenazine N atoms lowers the dark state below the bright state quenching the luminescence as a result of a rapid non-radiative decay pathway to the singlet ground state. McKinley *et al.* represented this schematically for $[\text{Ru}(\text{phen})_2\text{dppz}]^{2+}$ in which phen = 1,10 phenanthroline (**Fig. 7**):²²

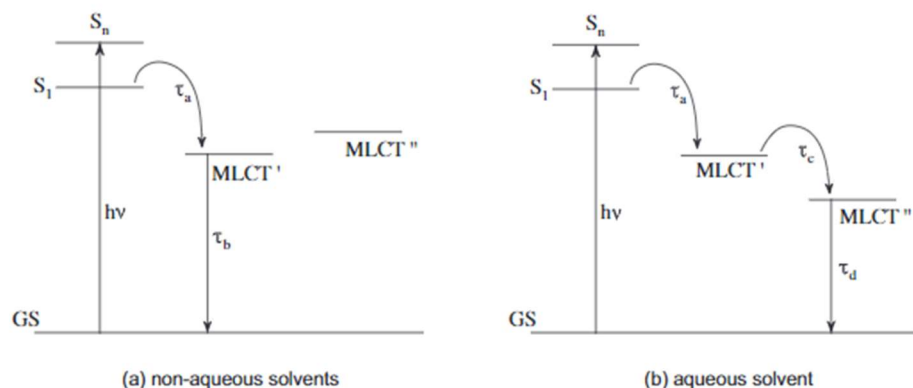


Fig. 7 Schematic representation of relative energies of states on dppz ligand involved in “light switch” effect in (a) non-aqueous solvents and (b) aqueous solvent: S_1 , S_n are the singlet excited states. GS is the singlet ground state. MLCT’ is the bright primary state associated with metal-to-ligand charge-transfer. MLCT’’ is the dark secondary state associated with metal-to-ligand charge-transfer. τ are luminescence lifetimes.

In the aqueous environment the dark secondary state dominates via a rapid (approximately 3ps) MLCT’ to MLCT’’ interconversion. Although the dark secondary state is emissive, it has a very low luminescence quantum yield due to its close proximity to the singlet ground state and the rapid non-radiative pathway which operates as a short-circuit to the GS. Therefore, the luminescence is not observed. However, structural and environmental changes which make the phenazine moiety less stable would raise the energy of the dark secondary state above that of the bright primary state shutting off the MLCT’ to MLCT’’ interconversion thus increasing the luminescence from the bright state. This could be caused by, for example, the presence of electron donating methyl groups at positions 10, 11, 12 or 13 on dppz (see **Fig. 5**) or the use of an aprotic solvent.

Brennaman *et al.* confirmed the existence of the two close and low-lying states on the dppz ligand but they found them to be photophysically similar to the triplet $^3\text{MLCT}$ state in $[\text{Ru}(\text{bpy})_3]^{2+}$.²³ They concluded, therefore, that both the bright and the dark states were $^3\text{MLCT}$ but their data were not consistent with the energy levels of the states being reversed to account for the “light switch” behaviour. Based on temperature dependence measurements they showed that the dark state was always lower than the bright state even in aprotic solvents and that the luminescence was determined by a dynamic equilibrium between the two states, the dark state being favoured by enthalpy/energy considerations and the bright state by entropy factors. They concluded that the bright state was a $^3\text{MLCT}$ state in which the photoexcited electron was located on the bpy section of the ligand and suggested that the dark state was also a $^3\text{MLCT}$ state but with a greater degree of charge-transfer character and situated on the phenazine part. This explains why the use of a more polar solvent lowers the luminescence as it would stabilize the dark state more and reduce the energy gap to the singlet ground state, thus making the non-radiative decay pathway more accessible.

Lowering the temperature would have a similar effect but a higher temperature increases entropy and favours the bright state which means greater luminescence. Equally, if a less polar solvent is used the dark state is not as stable and higher in terms of energy. The larger energy gap between the dark state and the singlet ground state would result in less non-radiative decay, increased back energy transfer and a population shift towards the bright state thereby resulting in increased luminescence (**Fig. 8(a)**). As before, electron donating methyl groups substituted onto the phenazine moiety would also destabilize the dark state and have the same effect. This was confirmed by Hartshorn and Barton in their measurements of the relative intensities of luminescence of $[\text{Ru}(\text{phen})_2\text{dppz}]^{2+}$ (0.56) and $[\text{Ru}(\text{phen})_2\text{dppx}]^{2+}$ (1.46) compared to $[\text{Ru}(\text{bpy})_3]^{2+}$ (dppx = 11,12-dimethyldipyridophenazine) (**Fig. 8(b)**).²⁴ Conversely, electron withdrawing groups would stabilize the dark state, increase the likelihood of the short circuit to the singlet ground state and lead to a lower emission intensity as shown in the work of McKinley *et al.* with bromination at positions 11 and 12 on dppz.²²

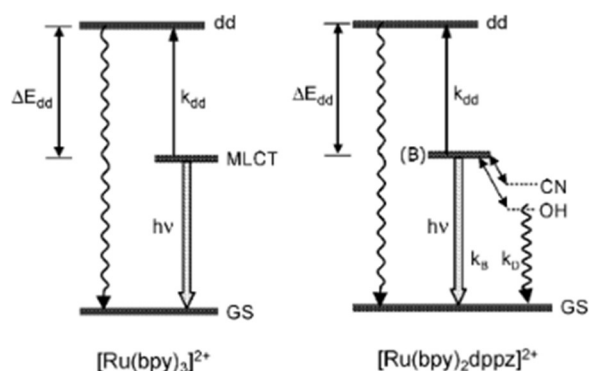


Fig. 8(a) $[\text{Ru}(\text{bpy})_2\text{dppz}]^{2+}$ “light switch” mechanism: dd are the ruthenium centred triplet ^3dd states. ΔE_{dd} is the energy gap from the bright state to the ^3dd states and k_{dd} is the rate at which this transition takes place. (B) is the bright state and CN is the dark state in an aprotic solvent such as acetonitrile whilst OH is the dark state in a protic solvent such as water. GS is the singlet ground state. k_{B} and k_{D} are the relaxation rates from the bright state and dark state respectively to GS.

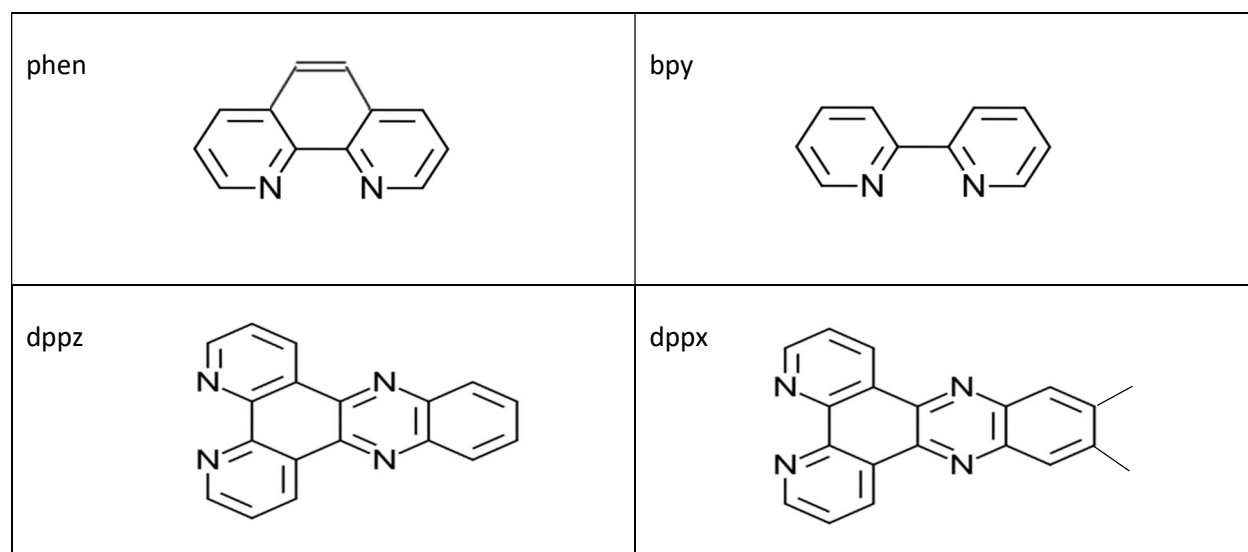


Fig 8(b) Structures of ligands involved in measurements of relative intensities of luminescence

Time-dependent Density Functional Theory calculations carried out by Sun *et al.* concluded that the electron density of the lowest unoccupied molecular orbital (LUMO) was located on the distal portion of dppz.¹³ Therefore, it is expected that transitions from the central Ru(II) dπ HOMO to this LUMO will result in non-emissive or weakly emissive MLCT states. This clearly equates to the ³MLCT dark excited state situated on the phenazine part of the ligand. The electron densities of the LUMO+1, LUMO+2 and LUMO+3 are localized on the proximal section of dppz which should be emissive and would be consistent with electron transfer from the central Ru(II) dπ HOMO to the bpy moiety of dppz or the ³MLCT bright excited state.

1.5 DNA and the “light switch” effect

Returning to the “light switch” effect of [Ru(bpy)₂dppz]²⁺ with DNA, the complex shows a brighter emission in the presence of a DNA mismatch compared to completely well-matched DNA base pairs.²⁵ In a similar way to the octahedral rhodium complexes, it has been shown to bind at the mismatch site through the minor groove through metalloinsertion. However, it readily binds to well-matched sites in the DNA duplex through intercalation as well.²⁶ Derivatives of the complex in which the inserting dppz functional group ligand has been functionalized by increasing steric bulk have been investigated but with no significant luminescence selectivity between the mismatched, abasic and well-matched DNA.²⁷ On the other hand, Boynton *et al.*¹² found that methylation of the bpy ancillary ligands in [Ru(bpy)₂dppz]²⁺ at the 5 and 5' positions resulted in a six-fold increase in the luminescence for a duplex containing a CC mismatch compared to a well-matched base pair. The main focus of their work was [Ru(Me₄phen)₂dppz]²⁺ (**Fig. 9**) for which they discovered a seven-fold luminescence enhancement for the same mismatch/well-matched base pair difference. The overall conclusion reached, therefore, was that increasing steric bulk of the ancillary ligand through methylation retained “light switch” behaviour but promoted mismatch selectivity.

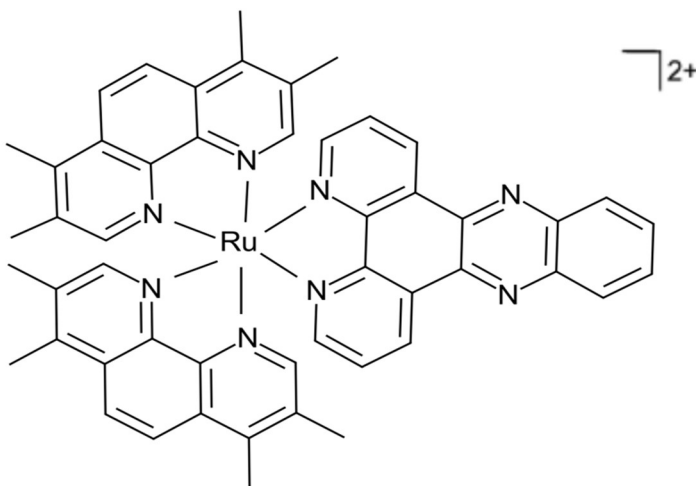


Fig. 9 Chemical structure of [Ru(Me₄phen)₂dppz]²⁺

In other work, Deraedt *et al.* reported that “elbow-shaped” intercalating functional group ligands such as benzodipyridophenazine (bdppz) (**Fig. 10**) were able to achieve noticeable luminescence signal enhancement for a mismatch compared to a well-matched sequence.⁴

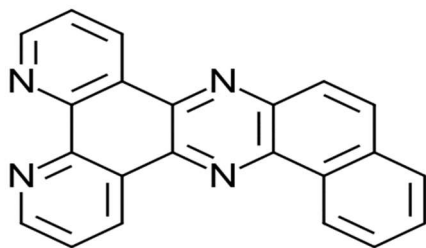


Fig. 10 Chemical structure of benzodipyridophenazine (bdppz) ligand.

Boynton *at al.* investigated another asymmetric, sterically expansive functional group ligand, benzonaphthyridine-1-isoquinoline (BNIQ) (**Fig.11**) and achieved high selectivity towards a CC mismatch or an abasic site compared to fully well-matched duplex DNA.⁹ Based on luminescence quenching experiments and the observation that the complex binds preferentially to more destabilized mismatch base pairings, they concluded that the mode of binding was metalloinsertion.

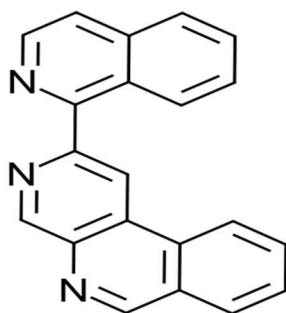


Fig. 11 Chemical structure of benzonaphthyridine-1-isoquinoline (BNIQ) ligand.

1.6 Aim of study

The aim of this study was to synthesize (**Schemes 1, 2, 3 and 4**) and then evaluate a series of eight ruthenium polypyridyl complexes (**Table 1**) for their ability to interact with DNA sequences containing a mismatch base pair. Although the ancillary and the functional group ligands have all been co-ordinated to ruthenium in previous work, five of the combinations used in this investigation are novel (**Table 4**). To improve the previous mismatch selectivity and enhance the brightness of the signal two strategies were considered:¹²

- (i) methylation of the ancillary bpy ligands and the dppz functional group ligand (**Fig. 5 and Table 1**);
- (ii) investigation of the “elbow-shaped” 12,17-dihydronaphthodipyridophenazine-12,17-dione (aqphen) functional group ligand (**Fig. 12 and Table 1**) along with methylation of the ancillary bpy ligands attached to this complex as well (**Fig. 13 and Table 1**):

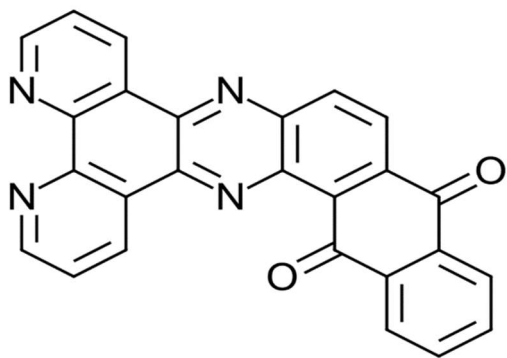


Fig. 12 Structure of 12,17-dihydro-1,2,17,18-diphenazepine-12,17-dione (aqphen) ligand.

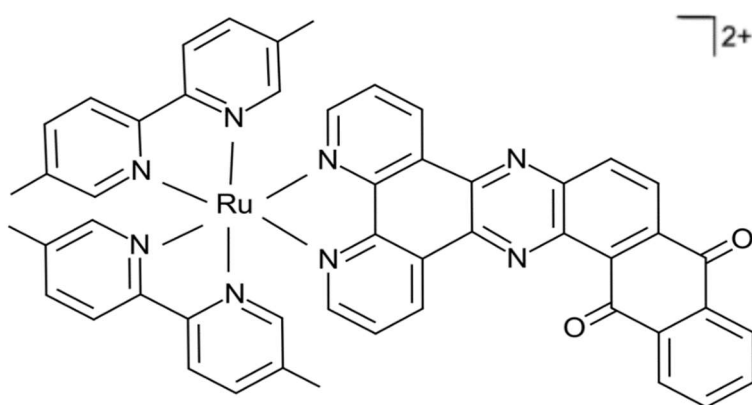


Fig. 13 Structure of $[Ru(5,5'\text{-dmbpy})_2(\text{aqphen})]^{2+}$

2. Experimental Procedures

2.1 Preparation of complexes

Materials

All reagents and solvents used were obtained from commercial sources, were at least reagent grade quality and were used without further purification.

Instrumentation

Mass Spectrometry

Samples were analysed at the EPSRC UK National Mass Spectrometry Facility at Swansea University using a ThermoScientific LTQ Orbitrap XL 1 Mass Spectrometer.

Infrared

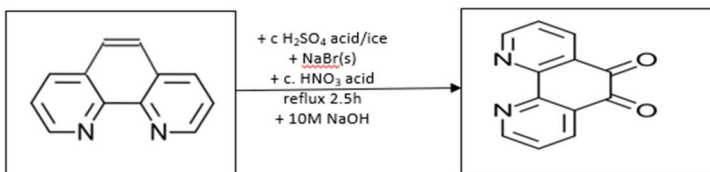
Fourier Transform Infrared Spectra were run on a Perkin Elmer FT-IR Spectrometer Spectrum TWO.

¹H NMR

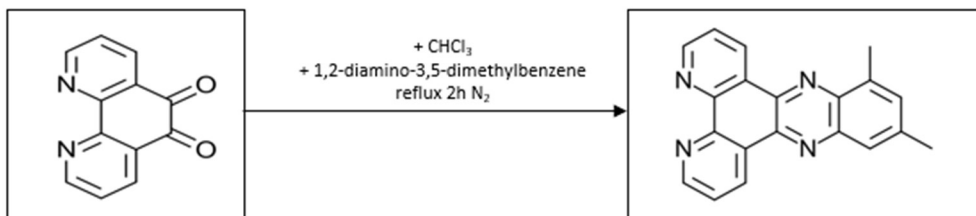
Spectra were obtained using a Bruker Advance III 500MHz Nuclear Magnetic Resonance Spectrometer.

Syntheses

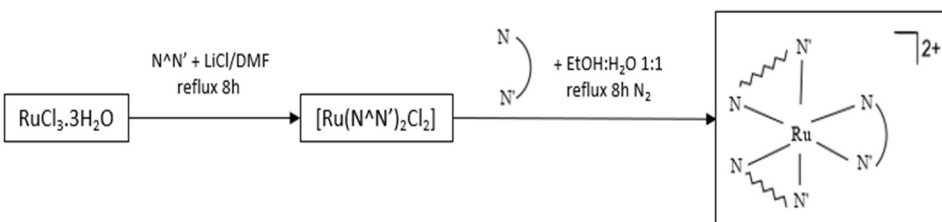
Scheme 1 – synthesis of 1,10-phenanthroline-5,6-dione (phendione or dpq)²⁸



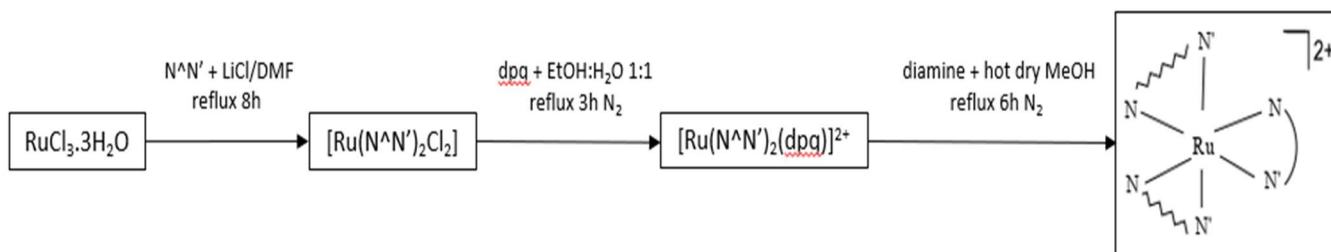
Scheme 2 – synthesis of 10,12-dimethyldipyridophenazine (dmdppz)²⁹




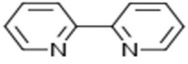
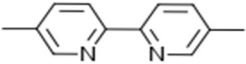
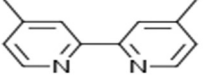
Scheme 3 – two step/direct route^{29,30}

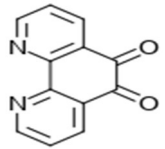


Scheme 4 – three step method^{29,30}



Key for Schemes 3 and 4

Ancillary ligand	$N \wedge N'$ 	bpy	
		5,5'-dmbpy	
		4,4'-dmbpy	

dpp or phendione	
---------------------	---

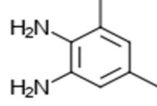
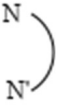
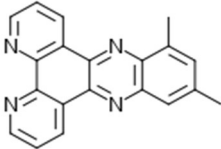
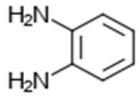
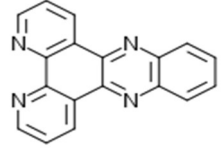
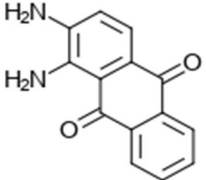
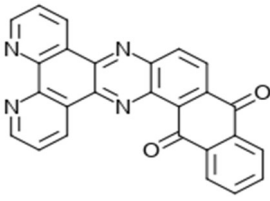
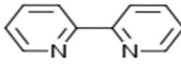
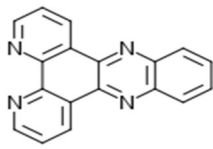
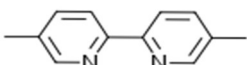
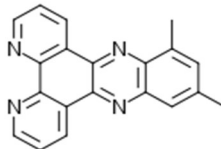
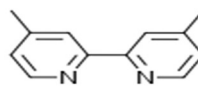
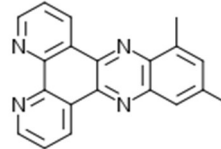
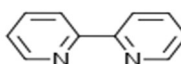
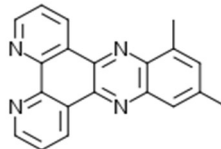
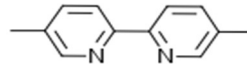
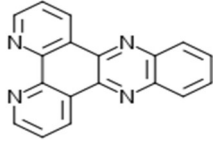
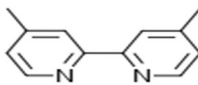
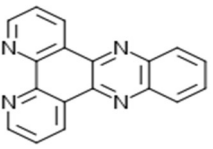
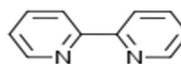
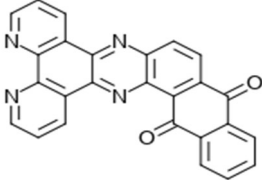
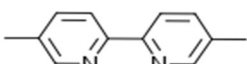
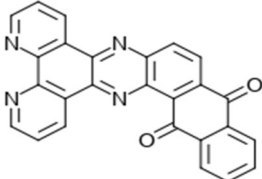
Diamine	1,2-diamino-3,5-dimethylbenzene		Functional group ligand	$N \wedge N'$ 	dmdppz	
	o-phenylenediamine				dppz	
	1,2-diaminoanthraquinone				aqphen	

Table 1. Complexes synthesized.

Target complex number		Ancillary ligand	Functional group ligand
1	$[\text{Ru}(\text{bpy})_2(\text{dppz})](\text{PF}_6)_2$		
2	$[\text{Ru}(5,5'\text{-dmbpy})_2(\text{dmdppz})](\text{PF}_6)_2$		
3	$[\text{Ru}(4,4'\text{-dmbpy})_2(\text{dmdppz})](\text{PF}_6)_2$		
4	$[\text{Ru}(\text{bpy})_2(\text{dmdppz})](\text{PF}_6)_2$		
5	$[\text{Ru}(5,5'\text{-dmbpy})_2(\text{dppz})](\text{PF}_6)_2$		
6	$[\text{Ru}(4,4'\text{-dmbpy})_2(\text{dppz})](\text{PF}_6)_2$		
7	$[\text{Ru}(\text{bpy})_2(\text{aqphen})](\text{PF}_6)_2$		
8	$[\text{Ru}(5,5'\text{-dmbpy})_2(\text{aqphen})](\text{PF}_6)_2$		

a) **1,10-Phenanthroline-5,6-dione (phendione or dpq) intermediate compound (i):**²⁸

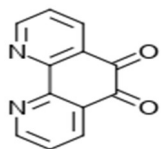


Fig. 14 Structure of dpq

5.12 g (28.4 mmol) of 1,10-phenanthroline was slowly added, with stirring, to 30 mL of concentrated sulphuric acid surrounded by ice. 2.55 g (25.0 mmol) of sodium bromide was added quickly followed by 15 mL of concentrated nitric acid. The mixture was allowed to reach room temperature before it was refluxed for 2.5 hours, allowing any bromine vapour to escape. The heating was then reduced to a lower intensity, the condenser removed and nitrogen gas used to speed up the removal of any residual bromine vapour.

The mixture was cooled to room temperature, poured onto approximately 400 g of crushed ice and, once the ice had melted, neutralized to pH 5/6 using a solution of 10 M sodium hydroxide. It was then left to stand for 30 minutes and vacuum filtered using a glass pad. 100 mL of boiling DI water was added to the filtrate before it was allowed to stand for a further 48 hours.

The aqueous solution was separated into two and the desired product extracted using dichloromethane (three 100 mL portions of dichloromethane for each aqueous half). The combined dichloromethane layers were washed with approximately 100 mL of DI water followed by approximately 50 mL of brine, dried over solid magnesium sulphate, and concentrated via rotatory evaporation.

The crude yellow product was recrystallized from a 50:1 methanol:DI water mixture to afford the title compound as a yellow solid.

Analysis

Yield: 2.07 g or 9.86 mmol (35 %). HRMS for $C_{12}H_6N_2O_2$: $[M+H]^+$ at 211.0501 and $[M+Na]^+$ at 233.0318. FTIR: 1414, 1461 and 1616 cm^{-1} . $^1\text{H NMR}$ (500 MHz, CDCl_3), δ , ppm: 9.13 (dd, $J = 1.8, 4.7\text{ Hz}$, 2H), 8.51 (dd, $J = 1.8, 7.8\text{ Hz}$, 2H), 7.59 (dd, $J = 4.4, 7.6\text{ Hz}$, 2H).

b) **10,12-Dimethyldipyridophenazine (dmdppz) intermediate compound (ii):**²⁹

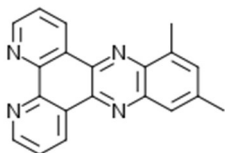


Fig. 15 Structure of dmdppz

0.349 g (1.66 mmol) of dpq was added to 17 mL of chloroform, followed by 0.237 g (1.74 mmol) of 1,2-diamino-3,5-dimethylbenzene. The mixture was refluxed under nitrogen gas for two hours, cooled to room temperature and the light yellow solid filtered, washed with ether, recrystallized using a hot dichloromethane:ethanol mixture (1:1) and then dried *in vacuo*.

Analysis

Yield: 0.243 g or 0.784 mmol (47 %). HRMS for $C_{20}H_{14}N_4$: $[M+H]^+$ at 311.1288 and $[M+Na]^+$ at 333.1106. FTIR: 1400 and 1479 cm^{-1} . 1H NMR (500 MHz, $CDCl_3$), δ , ppm: 9.72 (t, $J = 9.0$ Hz, 2H), 9.40 (s, 2H), 7.95 (s, 1H), 7.91 (dd, $J = 8.0, 4.6$ Hz, 2H), 7.61 (d, $J = 9.9$ Hz, 1H), 2.98 (s, 3H), 2.66 (s, 3H).

c) **[Ru(bpy)₂Cl₂] intermediate compound (iii):**³⁰

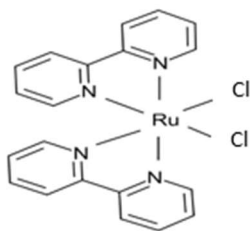


Fig. 16 Structure of $[Ru(bpy)_2Cl_2]$ where bpy = 2,2'-bipyridine.

0.543 g (2.08 mmol) of $RuCl_3 \cdot 3H_2O$, 0.646 g (4.14 mmol) of bpy and 0.611 g (14.6 mmol) of lithium chloride were dissolved in 10 mL of dimethylformamide (DMF) and the mixture refluxed for eight hours. After cooling to room temperature, 50mL of acetone was added, and the mixture cooled to 4 °C for 16 hours. The black precipitate formed was filtered, washed with DI water followed by ether before drying *in vacuo* and then in an oven for one hour.

Analysis

Yield: 0.680 g or 1.41 mmol (68 %). HRMS for $RuC_{20}H_{16}N_4Cl_2$: $[M+Na]^+$ at 506.9685.

d) $[\text{Ru}(5,5'\text{dmbpy})_2\text{Cl}_2]$ intermediate compound (iv):³⁰

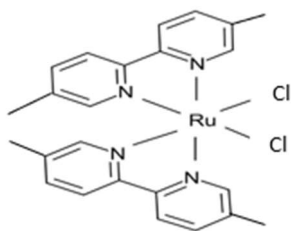


Fig. 17 Structure of $[\text{Ru}(5,5'\text{dmbpy})_2\text{Cl}_2]$ where 5,5'-dmbpy = 5,5'-dimethyl-2,2'-bipyridine.

Method as for **c**) using 1.13 g (4.33 mmol) of $\text{RuCl}_3 \cdot 3\text{H}_2\text{O}$, 1.64 g (8.90 mmol) of 5,5'-dmbpy and 1.33 g (31.4 mmol) of lithium chloride. A black precipitate was formed.

Analysis

Yield: 0.939 g or 1.74 mmol (40 %). HRMS for $\text{RuC}_{24}\text{H}_{24}\text{N}_4\text{Cl}_2$: $[\text{M}+\text{Na}]^+$ at 563.0308.

e) $[\text{Ru}(4,4'\text{dmbpy})_2\text{Cl}_2]$ intermediate compound (v):³⁰

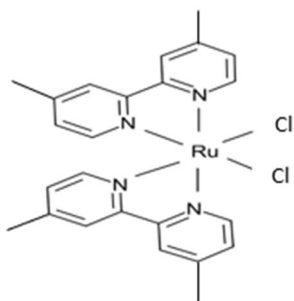


Fig. 18 Structure of $[\text{Ru}(4,4'\text{dmbpy})_2\text{Cl}_2]$ where 4,4'-dmbpy = 4,4'-dimethyl-2,2'-bipyridine.

Method as for **c**) using 0.480 g (1.84 mmol) of $\text{RuCl}_3 \cdot 3\text{H}_2\text{O}$, 0.697 g (3.79 mmol) of 4,4'-dmbpy and 0.587 g (14.0 mmol) of lithium chloride. A black precipitate was formed.

Analysis

Yield: 0.535 g or 0.99 mmol (54 %). HRMS for $\text{RuC}_{24}\text{H}_{24}\text{N}_4\text{Cl}_2$: $[\text{M}+\text{Na}]^+$ at 563.0319.

f) **[Ru(bpy)₂(dmdppz)](PF₆)₂ (two step/direct route – see Scheme 3) target complex 4:**²⁹

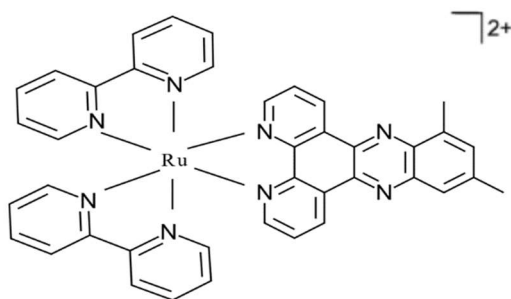


Fig. 19 Structure of [Ru(bpy)₂(dmdppz)]²⁺

0.256 g (0.529 mmol) of [Ru(bpy)₂Cl₂] was added to 27 mL of a mixture of ethanol:water 1:1, followed by 0.165 g (0.532 mmol) of dmdppz. The mixture was refluxed under nitrogen gas for eight hours, cooled to room temperature and then cooled at 4 °C for 16 hours. The brown solution was filtered and the ethanol removed by rotatory evaporation. 1 mL of a saturated aqueous solution of ammonium hexafluorophosphate was added and the dark brown precipitate formed collected via filtration. The precipitate was washed with DI water and recrystallized from acetonitrile, the filtrate being added to 30 mL of ether in an ice-bath to aid crystal formation. The bright orange solid formed was collected via filtration, washed with ether and dried *in vacuo*.

Analysis

Yield: 0.253 g or 0.249 mmol (47 %). HRMS for RuC₄₀H₃₀N₈P₂F₁₂: [M - 2PF₆]²⁺ at 362.0818 and [M - PF₆]⁺ at 869.1284. FTIR: 556, 831, 1447 and 1464 cm⁻¹. ¹H NMR (500 MHz, D₆ acetone), δ, ppm: 9.82 (dd, *J* = 8.2, 1.1 Hz, 1H), 9.74 (dd, *J* = 8.2, 1.1 Hz, 1H), 8.87 (dd, *J* = 17.6, 8.2 Hz, 4H), 8.54 (ddd, *J* = 10.4, 5.3, 1.2 Hz, 2H), 8.28 (d, *J* = 8.0 Hz, 2H), 8.12 (m, 9H), 7.90 (s, 1H), 7.66 (m, 2H), 7.42 (m, 2H), 3.03 (s, 3H), 2.72 (s, 3H). Data confirmed purity of complex 4 synthesised via the two step/direct route.

g) **[Ru(bpy)₂(dpq)](PF₆)₂ (three step method – see Scheme 4) intermediate compound (vi):**²⁹

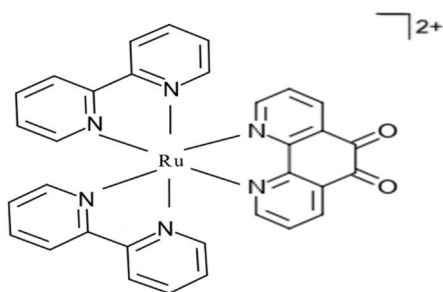


Fig. 20 Structure of [Ru(bpy)₂(dpq)]²⁺

0.382 g (0.789 mmol) of $[\text{Ru}(\text{bpy})_2\text{Cl}_2]$ and 0.166 g (0.790 mmol) of dpq were purged with nitrogen gas and added to 20 mL of a mixture of ethanol:water 1:1 which had been flushed with nitrogen gas. The mixture was refluxed under nitrogen gas for three hours before being allowed to cool to room temperature. 1 mL of a saturated aqueous solution of ammonium hexafluorophosphate was added and the brown precipitate formed collected via filtration, washed with DI water followed by ether before drying *in vacuo* and then in an oven for 48 hours.

Analysis

Yield: 0.561 g or 0.614 mmol (78 %). FTIR: 556, 831, 1426, 1444, 1448 and 1699 cm^{-1} . ^1H NMR (500 MHz, D6 acetone), δ , ppm: 8.85 (d, $J = 8.0$ Hz, 4H), 8.65 (dd, $J = 7.9, 1.1$ Hz, 2H), 8.38 (d, $J = 5.6$ Hz, 2H), 8.25 (t, $J = 7.9$ Hz, 4H), 8.12 (m, 4H), 7.83 (dd, $J = 7.9, 5.6$ Hz, 2H), 7.60 (m, 4H).

h) $[\text{Ru}(5,5'\text{dmbpy})_2(\text{dpq})](\text{PF}_6)_2$ intermediate compound (vii):²⁹

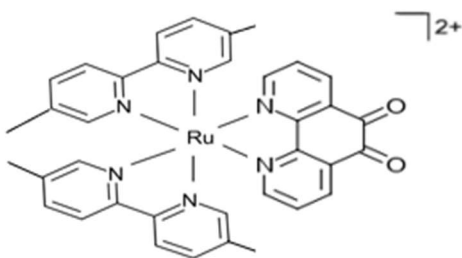


Fig. 21 Structure of $[\text{Ru}(5,5'\text{dmbpy})_2(\text{dpq})]^{2+}$

Method as for **g**) using 0.677 g (1.25 mmol) of $[\text{Ru}(5,5'\text{dmbpy})_2\text{Cl}_2]$ and 0.262 g (1.25 mmol) of dpq. A brown precipitate was formed.

Analysis

Yield: 1.13 g or 1.16 mmol (93 %). FTIR: 556, 835, 1428, 1477 and 1699 cm^{-1} . ^1H NMR (500 MHz, D6 acetone), δ , ppm: 8.65 (d, $J = 8.4$ Hz, 4H), 8.62 (m, 2H), 8.34 (dd, $J = 5.6, 1.2$ Hz, 2H), 8.03 (d, $J = 8.3$ Hz, 4H), 7.89 (d, $J = 35.2$ Hz, 4H), 7.80 (m, 2H), 2.22 (s, 6H), 2.17 (s, 6H).

i) $[\text{Ru}(4,4'\text{dmbpy})_2(\text{dpq})](\text{PF}_6)_2$ intermediate compound (viii):²⁹

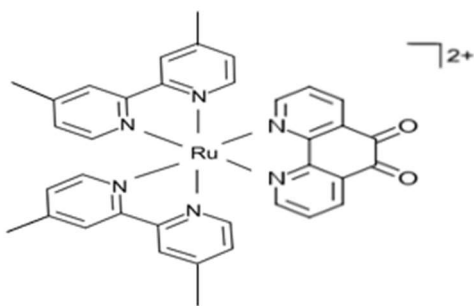


Fig. 22 Structure of $[\text{Ru}(4,4'\text{dmbpy})_2(\text{dpq})]^{2+}$

Method as for **g**) using 0.400 g (0.741 mmol) of $[\text{Ru}(4,4'\text{-dmbpy})_2\text{Cl}_2]$ and 0.171 g (0.814 mmol) of dpq. A brown precipitate was formed.

Analysis

Yield: 0.708 g or 0.740 mmol (99 %). FTIR: 557, 826, 1427 and 1704 cm^{-1} . ^1H NMR (500 MHz, D6 acetone), δ , ppm: 8.69 (s, 4H), 8.60 (d, $J = 6.9$ Hz, 2H), 8.34 (m, 2H), 7.94 (d, $J = 5.8$ Hz, 2H), 7.86 (d, $J = 5.8$ Hz, 2H), 7.79 (m, 2H), 7.42 (d, $J = 5.9$ Hz, 2H), 7.38 (d, $J = 5.4$ Hz, 2H), 2.58 (s, 6H), 2.56 (s, 6H).

j) $[\text{Ru}(\text{bpy})_2(\text{dmdppz})](\text{PF}_6)_2$ (three step method – see Scheme 4) target complex 4.²⁹

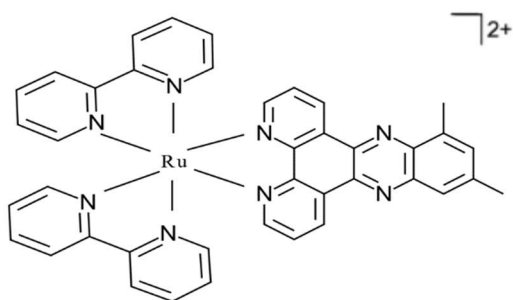


Fig. 19 Structure of $[\text{Ru}(\text{bpy})_2(\text{dmdppz})]^{2+}$

0.153 g (1.12 mmol) of 1,2-diamino-3,5-dimethylbenzene was dissolved in 25 mL of hot, anhydrous methanol (dried using solid magnesium sulphate). 0.212 g (0.232 mmol) of $[\text{Ru}(\text{bpy})_2(\text{dpq})](\text{PF}_6)_2$ was also dissolved in 25 mL of anhydrous methanol and the solution boiled before the first solution was added to it. The mixture was refluxed for six hours under nitrogen gas and allowed to cool to room temperature. 1 mL of a saturated aqueous solution of ammonium hexafluorophosphate was added to it and the mixture cooled in ice. The bright orange precipitate formed was collected by filtration and recrystallized from acetonitrile, the filtrate being added to 30 mL of ether in an ice-bath to aid crystal formation. The crystals formed were collected by filtration, washed with ether and dried in an oven.

Analysis

Yield: 0.164 g or 0.162 mmol (70 %). HRMS for $\text{RuC}_{40}\text{H}_{30}\text{N}_8\text{P}_2\text{F}_{12}$: $[\text{M} - 2\text{PF}_6]^{2+}$ at 362.0814 and $[\text{M} - \text{PF}_6]^+$ at 869.1272. FTIR: 557, 836 and 1447 cm^{-1} . ^1H NMR (500 MHz, D6 acetone), δ , ppm: 9.82 (s, 1H), 9.75 (d, $J = 7.1$ Hz, 1H), 8.88 (d, $J = 9.5$ Hz, 4H), 8.54 (dd, $J = 7.7, 2.7$ Hz, 2H), 8.29 (s, 2H), 8.15 (m, 9H), 7.90 (s, 1H), 7.67 (s, 2H), 7.43 (d, $J = 1.4$ Hz, 2H), 3.03 (s, 3H), 2.72 (s, 3H). Data confirmed purity of complex 4 synthesised via the three step method.

k) **[Ru(5,5'dmbpy)₂(dmdppz)](PF₆)₂ target complex 2:**²⁹

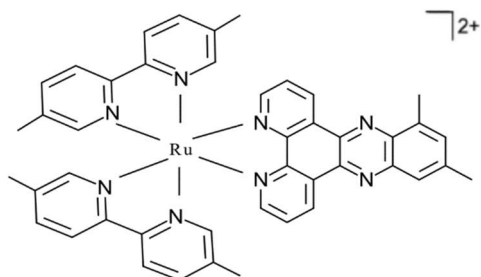


Fig. 23 Structure of [Ru(5,5'dmbpy)₂(dmdppz)]²⁺

Method as for **j**) using 0.242 g (0.249 mmol) of [Ru(5,5'dmbpy)₂(dpq)](PF₆)₂ and 0.148 g (1.09 mmol) of 1,2-diamino-3,5-dimethylbenzene. An orange precipitate was formed. TLC analysis of the product (R_f = 0.88) on alumina plates using pure acetonitrile as the mobile phase revealed that it was a mixture and so column chromatography, using the same stationary phase and a 1:1 mixture of acetonitrile and toluene as the solvent, was used to separate it from the other components present.

Analysis

Yield: 0.233 g or 0.218 mmol (87 %). HRMS for RuC₄₄H₃₈N₈Cl₂: [M – 2Cl]²⁺ at 390.1123. FTIR: 557, 837 and 1477 cm⁻¹. ¹H NMR (500 MHz, D₆ acetone), δ, ppm: 9.78 (d, J = 7.2 Hz, 1H), 9.70 (m, 1H), 8.69 (d, J = 8.4 Hz, 2H), 8.65 (d, J = 8.3 Hz, 2H), 8.60 (t, J = 6.4 Hz, 2H), 8.49 (dd, J = 6.0, 2.7 Hz, 2H), 8.07 (d, J = 6.8 Hz, 3H), 7.97 (s, 1H), 7.87 (s, 2H), 7.23 (s, 2H), 7.18 (s, 2H), 3.03 (s, 3H), 2.71 (s, 3H), 2.27 (s, 6H), 2.02 (s, 6H). Data confirmed purity of complex 2 synthesised via the three step method.

l) **[Ru(4,4'dmbpy)₂(dmdppz)](PF₆)₂ target complex 3:**²⁹

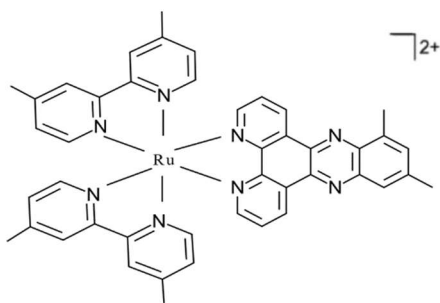


Fig. 24 Structure of [Ru(4,4'dmbpy)₂(dmdppz)]²⁺

Method as for **j**) using 0.610 g (0.629 mmol) of [Ru(4,4'dmbpy)₂(dpq)](PF₆)₂ and 0.178 g (1.31 mmol) of 1,2-diamino-3,5-dimethylbenzene. An orange-brown precipitate was formed.

Analysis

Yield: 0.544 g or 0.508 mmol (81 %). HRMS for $\text{RuC}_{44}\text{H}_{38}\text{N}_8\text{Cl}_2$: $[\text{M} - 2\text{Cl}]^{2+}$ at 390.1130. FTIR: 556, 840 and 1414 cm^{-1} . $^1\text{H NMR}$ (500 MHz, D_6 acetone), δ , ppm: 9.76 (d, $J = 7.6\text{ Hz}$, 1H), 9.69 (d, $J = 8.1\text{ Hz}$, 1H), 8.74 (s, 2H), 8.70 (s, 2H), 8.51 (m, 2H), 8.08 (d, $J = 6.2\text{ Hz}$, 2H), 8.05 (m, 2H), 7.98 (dd, $J = 5.7, 1.8\text{ Hz}$, 2H), 7.88 (d, $J = 2.8\text{ Hz}$, 2H), 7.48 (d, $J = 5.6\text{ Hz}$, 2H), 7.23 (d, $J = 5.9\text{ Hz}$, 2H), 3.02 (s, 3H), 2.71 (s, 3H), 2.62 (s, 6H), 2.51 (s, 6H). Data confirmed purity of complex 3 synthesised via the three step method.

m) $[\text{Ru}(\text{bpy})_2(\text{dppz})](\text{PF}_6)_2$ target complex 1:²⁹

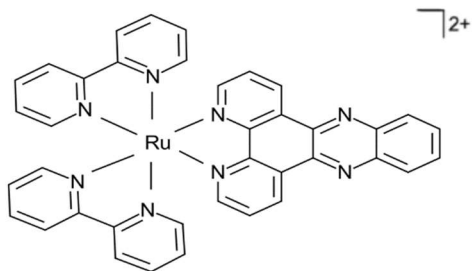


Fig. 25 Structure of $[\text{Ru}(\text{bpy})_2(\text{dppz})]^{2+}$ where dppz = dipyrrophenazine.

Method as for **j**) using 0.497 g (0.544 mmol) of $[\text{Ru}(\text{bpy})_2(\text{dpq})](\text{PF}_6)_2$ and 0.124 g (1.15 mmol) o-phenylenediamine. A bright orange precipitate was formed.

Analysis

Yield: 0.188 g or 0.191 mmol (35 %). HRMS for $\text{RuC}_{38}\text{H}_{26}\text{N}_8\text{Cl}_2$: $[\text{M} - 2\text{Cl}]^{2+}$ at 348.0660. FTIR: 555, 831, 1422 and 1448 cm^{-1} . $^1\text{H NMR}$ (500 MHz, D_6 acetone), δ , ppm: 9.78 (d, $J = 1.2\text{ Hz}$, 2H), 8.88 (s, 2H), 8.85 (s, 2H), 8.56 (m, 2H), 8.52 (m, 2H), 8.29 (td, $J = 8.0, 1.4\text{ Hz}$, 4H), 8.20 (d, $J = 5.0\text{ Hz}$, 4H), 8.12 (d, $J = 5.4\text{ Hz}$, 4H), 7.66 (dd, $J = 4.2, 2.7\text{ Hz}$, 2H), 7.42 (d, $J = 5.7\text{ Hz}$, 2H). Data confirmed purity of complex 1 synthesised via the three step method.

n) $[\text{Ru}(5,5'\text{-dmbpy})_2(\text{dppz})](\text{PF}_6)_2$ target complex 5.²⁹

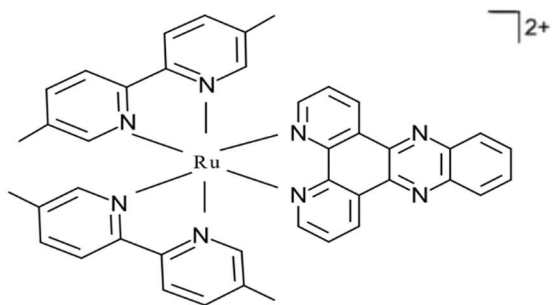


Fig. 26 Structure of $[\text{Ru}(5,5'\text{-dmbpy})_2(\text{dppz})]^{2+}$

Method as for **j**) using 0.508 g (0.524 mmol) of $[\text{Ru}(5,5'\text{-dmbpy})_2(\text{dpq})](\text{PF}_6)_2$ and 0.128 g (1.18 mmol) o-phenylenediamine. An orange precipitate was formed. TLC analysis of the product ($R_f = 0.93$) on alumina plates using a 9:1 mixture of acetonitrile and water as the mobile phase revealed that it was a mixture and so column chromatography, using the same stationary phase and a 2:1 mixture of acetonitrile and toluene as the solvent, was used to separate it from the other components present.

Analysis

Yield: 0.446 g or 0.428 mmol (82 %). HRMS for $\text{RuC}_{42}\text{H}_{34}\text{N}_8\text{Cl}_2$: $[\text{M} - 2\text{Cl}]^{2+}$ at 376.0972. FTIR: 556, 833 and 1474 cm^{-1} . $^1\text{H NMR}$ (500 MHz, D_6 acetone), δ , ppm: 9.74 (d, $J = 1.1\text{ Hz}$, 2H), 8.70 (d, $J = 8.4\text{ Hz}$, 2H), 8.65 (s, 2H), 8.53 (d, $J = 3.0\text{ Hz}$, 2H), 8.51 (m, 2H), 8.22 (dd, $J = 6.5, 3.4\text{ Hz}$, 2H), 8.09 (d, $J = 5.4\text{ Hz}$, 2H), 8.07 (s, 2H), 7.97 (s, 2H), 7.87 (s, 2H), 7.20 (dd, $J = 28.4, 7.4\text{ Hz}$, 2H), 2.27 (s, 6H), 2.01 (s, 6H). Data confirmed purity of complex 5 synthesised via the three step method.

o) $[\text{Ru}(4,4'\text{-dmbpy})_2(\text{dppz})](\text{PF}_6)_2$ target complex 6.²⁹

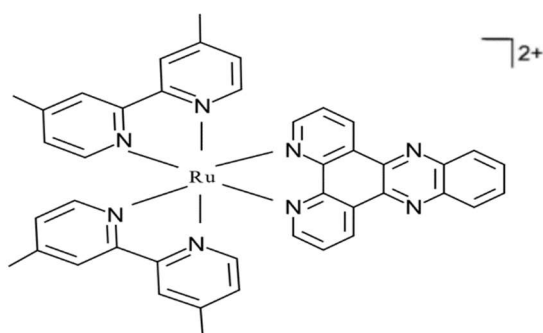


Fig. 27 Structure of $[\text{Ru}(4,4'\text{-dmbpy})_2(\text{dppz})]^{2+}$

Method as for **j**) using 0.203 g (0.209 mmol) of $[\text{Ru}(4,4'\text{-dmbpy})_2(\text{dpq})](\text{PF}_6)_2$ and 0.0516 g (0.477 mmol) o-phenylenediamine. An orange-brown precipitate was formed.

Analysis

Yield: 0.145 g or 0.139 mmol (66 %). HRMS for $\text{RuC}_{42}\text{H}_{34}\text{N}_8\text{Cl}_2$: $[\text{M} - 2\text{Cl}]^{2+}$ at 376.0971. FTIR: 556, 833, 1420 and 1482 cm^{-1} . $^1\text{H NMR}$ (500 MHz, D6 acetone), δ , ppm: 9.74 (dd, $J = 8.2, 1.2\text{ Hz}$, 2H), 8.75 (s, 2H), 8.70 (s, 2H), 8.55 (dd, $J = 5.3, 1.2\text{ Hz}$, 2H), 8.51 (dd, $J = 6.5, 3.4\text{ Hz}$, 2H), 8.21 (dd, $J = 6.4, 3.2\text{ Hz}$, 2H), 8.08 (m, 2H), 7.99 (d, $J = 5.7\text{ Hz}$, 2H), 7.89 (d, $J = 5.9\text{ Hz}$, 2H), 7.48 (d, $J = 4.8\text{ Hz}$, 2H), 7.23 (d, $J = 5.8\text{ Hz}$, 2H), 2.62 (s, 6H), 2.52 (d, $J = 6.8\text{ Hz}$, 6H). Data confirmed purity of complex 6 synthesised via the three step method.

p) $[\text{Ru}(\text{bpy})_2(\text{aqphen})](\text{PF}_6)_2$ target complex 7:²⁹

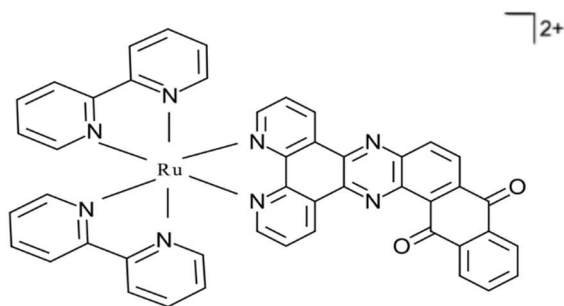


Fig. 28 Structure of $[\text{Ru}(\text{bpy})_2(\text{aqphen})]^{2+}$ where aqphen = 12,17-dihydronaphthodipyridophenazine-12,17-dione.

Method as for **j**) using 0.506 g (0.554 mmol) of $[\text{Ru}(\text{bpy})_2(\text{dpq})](\text{PF}_6)_2$ and 0.270 g (1.13 mmol) of 1,2-diaminoanthraquinone. An orange precipitate was formed. TLC analysis of the product ($R_f = 0.26$) on alumina plates using a mixture of 70:29:1 acetonitrile:water:saturated aqueous potassium nitrate solution as the mobile phase revealed that it was a mixture and so column chromatography, using the same stationary phase and pure acetonitrile as the solvent, was used to separate it from the other components present.

Analysis

Yield: 0.543 g or 0.487 mmol (88 %). HRMS for $\text{RuC}_{46}\text{H}_{28}\text{N}_8\text{O}_2\text{Cl}_2$: $[\text{M} - 2\text{Cl}]^{2+}$ at 413.0686. FTIR: 557, 836, 1421, 1447 and 1674 cm^{-1} . $^1\text{H NMR}$ (500 MHz, D6 acetone), δ , ppm: 9.91 (d, $J = 7.2\text{ Hz}$, 1H), 9.82 (d, $J = 8.0\text{ Hz}$, 1H), 8.91 (m, 5H), 8.64 (d, $J = 5.3\text{ Hz}$, 2H), 8.38 (dd, $J = 25.6, 7.3\text{ Hz}$, 3H), 8.30 (m, 2H), 8.19 (m, 7H), 8.03 (m, 3H), 7.68 (s, 2H), 7.44 (m, 2H). Data confirmed purity of complex 7 synthesised via the three step method.

q) **[Ru(5,5'dmbpy)₂(aqphen)](PF₆)₂ target complex 8:²⁹**

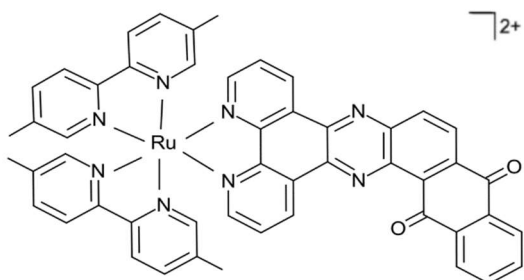


Fig. 29 Structure of [Ru(5,5'dmbpy)₂(aqphen)]²⁺

Method as for **j**) using 0.527 g (0.543 mmol) of [Ru(5,5'dmbpy)₂(dpq)](PF₆)₂ and 0.256 g (1.07 mmol) of 1,2-diaminoanthraquinone. A dark red-orange precipitate was formed. TLC analysis of the product (R_f = 0.80) on alumina plates using a 8:2 mixture of acetonitrile and water as the mobile phase revealed that it was a mixture and so column chromatography, using the same stationary phase and pure acetonitrile as the solvent, was used to separate it from the other components present.

Analysis

Yield: 0.422 g or 0.360 mmol (66 %). HRMS for RuC₅₀H₃₆N₈O₂Cl₂: [M – 2Cl]²⁺ at 441.0998. FTIR: 557, 836, 1477 and 1672 cm⁻¹. ¹H NMR (500 MHz, D₆ acetone), δ, ppm: 9.71 (d, J = 8.1 Hz, 1H), 9.64 (d, J = 8.1 Hz, 1H), 8.79 (m, 2H), 8.68 (dd, J = 8.7, 7.4 Hz, 5H), 8.57 (dd, J = 7.2, 2.8 Hz, 3H), 8.24 (s, 1H), 8.19 (s, 1H), 8.06 (m, 5H), 7.98 (s, 5H), 2.29 (s, 3H), 2.29 (s, 3H), 2.18 (m, 3H), 2.09 (s, 3H). Data confirmed purity of complex 8 synthesised via the three step method.

r) Preparation of chloride salts from hexafluorophosphate salts via counterion exchange

All eight of the ruthenium complexes prepared were converted into chloride salts by dissolving the hexafluorophosphate salt in the minimum quantity of acetone and adding an excess of a saturated solution of tetrabutylammonium chloride in acetone. The mixture was stored at 4 °C overnight and the precipitate of the chloride salt subsequently formed collected via vacuum filtration. The solid was then washed with acetone followed by ether before drying in an oven.

2.2 Photophysical characterization

Instrumentation

UV/VIS spectrometry

Spectra were obtained using a Perkin Elmer UV/VIS Lambda 365 Spectrometer.

Luminescence emission and excitation spectrometry

Spectra were run on a Perkin Elmer Fluorescence Spectrometer LS 55.

a) UV/VIS absorption spectra

Each ruthenium complex was dissolved in acetonitrile at a concentration of approximately 10 μM and 3 mL of the solution placed in a quartz glass cuvette. Spectra were run from 200 nm to 700 nm.

b) Luminescence Quantum Yields

A stock solution in acetonitrile of each ruthenium complex was prepared at a concentration of approximately 1 mM. A reference solution of $[\text{Ru}(\text{bpy})_3](\text{PF}_6)_2$ in the same solvent and at the same concentration was also prepared. 30 μL of the reference solution was added to 3 mL of acetonitrile in the cuvette and a UV/VIS spectrum run. This was repeated with 3 mL of acetonitrile and 20 μL of reference solution and, finally, 3 mL of acetonitrile and 10 μL of reference solution. The absorbances at 450 nm were noted. The same procedure was then carried out for all eight of the ruthenium complexes prepared.

Emission and excitation spectra were obtained using the same solutions. For the emission spectra, an excitation wavelength of 450 nm was used and the emission intensities measured from 500 nm to 750 nm. The integrated luminescence intensity was then calculated from the area under the curve. For the excitation spectra, the emission wavelength was determined by the emission spectra but it was approximately 600-623 nm; the excitation emission intensities were measured from 280 nm to 500 nm. The aqphen ligand in complexes has been reported as non-emissive in both aprotic and protic solvents^{16,31} and this was checked by carrying out the process in acetonitrile and then in DI water for complexes 7 and 8.

Luminescence Quantum Yields were calculated using the following equation:³²

Equation 1

$$Q_s = Q_r \left(\frac{A_r}{A_s} \right) \left(\frac{E_s}{E_r} \right) \left(\frac{n_s}{n_r} \right)^2$$

where:

Q = Luminescence Quantum Yield.

n = Refractive index of solvent.

A = Absorbance of solution.

E = Integrated luminescence intensity of emitted light.

subscript s refers to ruthenium complex.

subscript r refers to reference fluorophore.

As the same solvent is used for the ruthenium complex and the reference fluorophore $\left(\frac{n_s}{n_r}\right)^2 = 1$.

The gradient m of a calibration curve obtained by plotting integrated luminescence intensity on the y axis and absorbance on the x axis enables the equation to be simplified:

Equation 2

$$Q_s = Q_r \left(\frac{m_s}{m_r}\right)$$

which means that the Luminescence Quantum Yield can be calculated from the product of the Luminescence Quantum Yield of the reference and the quotient of the two gradients.

For $[\text{Ru}(\text{bpy})_3]^{2+}$:

$$Q_r = 0.018 \pm 0.002 \text{ at } \lambda_{\text{ex}} = 450\text{nm in acetonitrile.}^{33}$$

$$Q_r = 0.040 \pm 0.002 \text{ at } \lambda_{\text{ex}} = 450\text{nm in water.}^{33}$$

2.3 DNA binding studies

Materials

Solid chloride salts of ruthenium complexes 1 to 8.

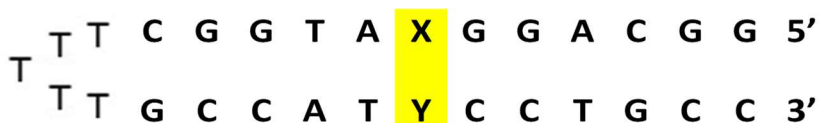
Tris = Tris Hydrochloride buffer containing 5 mM Tris Hydrochloride and 25 mM sodium chloride with a pH = 7.00 at 298 K.

PBS = Phosphate Buffered Saline solution containing 10 mM PBS, 2.7 mM potassium chloride and 137 mM sodium chloride with a pH = 7.40 at 298 K.

CT DNA = DNA sodium salt from calf-thymus.

Hairpin DNA with well-matched and mismatched base pairs: 10 in total (**Table 2**).

Table 2. Hairpin DNA sequences.



X	G	A	A	C	G	T	A	C	C	G
Y	C	T	A	C	G	T	G	A	T	T
	well-matched		mismatched							

12mer DNA = 12 base oligonucleotide duplex DNA. Two types: one with all well-matched base pairs and one with one CC mismatched base pair (**Table 3**). The duplexes were prepared by annealing: each oligonucleotide sequence was diluted to the required concentrations (12 μ M and 40 μ M) in the buffer, equal volumes mixed and, after a brief vortex, the mixture heated to 95 °C on a heating block for 5 minutes before being allowed to cool slowly to room temperature.³⁴

Table 3. 12mer DNA sequences.

3'	C	G	G	T	A	X	G	G	A	C	G	G	5'
5'	G	C	C	A	T	Y	C	C	T	G	C	C	3'
X	G	C											
Y	C	C											
	well-matched		mismatched										

EthBr = ethidium bromide stock solution prepared in Tris at a concentration of 5.48mM.

Instrumentation

UV/VIS spectrometry

Spectra were obtained using a Perkin Elmer UV/VIS Lambda 365 Spectrometer.

Luminescence emission spectrometry

Spectra were run either on a Perkin Elmer Fluorescence Spectrometer LS 55 or on a Tecan Infinite 200 PRO M Nano+ plate reader.

CT DNA

10 mg of CT DNA were added to 2 mL of Tris buffer solution. The mixture was vortexed until the CT DNA dissolved and then sonicated for 2x 15mins. Absorbances at 260 nm and at 280 nm were measured using a UV/VIS spectrometer to check the purity of the CT DNA solution. The threshold for purity used was $A_{260}/A_{280} > 1.8$.³⁵ The concentration of the CT DNA solution was determined from the following equation:

Equation 3

$$[DNA] = \frac{A_{260}}{\epsilon_{260}}$$

where ϵ_{260} = Extinction Coefficient at 260 nm = $6600 \text{ dm}^3 \text{ mol}^{-1} \text{ cm}^{-1}$.³⁵

This procedure was repeated using PBS buffer solution.

a) Luminescence titrations with complexes 1 to 6³⁶

Solutions of the chloride salt of each complex were made up in Tris buffer at a concentration of 3 μM and 3 mL of this solution were placed in the quartz glass cuvette. It was estimated from the literature that a concentration of 80 μM CT DNA solution in the cuvette would be required to remove all the quenching by water and, therefore, produce the maximum emission intensity.³⁷ This equated to between 18 μL and 24 μL of the stock CT DNA solution and so 2 μL aliquots were added to the cuvette with 2 minute equilibration times after each aliquot addition. At least 20 data points before the emission intensity reached a maximum were obtained. Luminescence emission spectra were run using an excitation wavelength of 450 nm and the emission intensities were measured from 500 nm to 800 nm.

Curves showing the fraction of complex bound to DNA versus $[DNA]/[\text{complex}]$ were used to generate Scatchard plots via SigmaPlot software.^{38,39} The fraction bound was calculated using the area under the emission curves as well as using the maximum emission intensities. The SigmaPlot software was then used to fit the McGhee-von Hippel equation to the Scatchard plots enabling binding constants K_b and site sizes (number of base pairs per site) n to be calculated.⁴⁰

The process was repeated in PBS buffer for comparative purposes.

b) UV/VIS titrations with complexes 1, 7 and 8^{41,42}

Solutions of the chloride salt of each complex were made up in Tris buffer at a concentration of 30 μM and 3 mL of this solution was placed in the quartz glass cuvette. 4 minute equilibration times after each aliquot addition of the stock solution of CT DNA were used and at least 20 data points before the absorbance curves reached a minimum were obtained. UV/VIS spectra were run from 200 nm to 700 nm.

Curves showing the fraction of complex bound to DNA versus $[\text{DNA}]/[\text{complex}]$ were used to generate Scatchard plots via SigmaPlot software. The fraction bound was calculated using the decrease in absorbance at approximately 290 nm. The SigmaPlot software was then used to fit the McGhee-von Hippel equation to the Scatchard plots enabling binding constants K_b and site sizes (number of base pairs per site) n to be calculated.

c) Luminescence via competitive displacement of ethidium bromide using complexes 1, 5, 7 and 8⁴³

A working solution of 20 μM CT DNA and 7 μM EthBr in Tris buffer was prepared by mixing together equal volumes of double the required concentrations of these solutions. Stock solutions of the chloride salt of each complex were prepared in Tris buffer at 2, 5, 10, 20, 50 and 100 μM .

50 μL of the CT DNA-EthBr working solution was placed in each well of a 96 well microplate with the exception of the reference wells to which 50 μL of Tris were added. 50 μL of the stock solutions of the complexes were then added to give final concentrations in the wells of 10 μM CT DNA, 3.5 μM EthBr and 1, 2.5, 5, 10, 25 and 50 (all μM) for the complexes. In the first row 50 μL of Tris were added instead of the complexes to achieve the required concentrations of the CT DNA and EthBr at 0 μM for each complex. The plate was shielded from light and allowed to incubate at room temperature for one hour before being analysed using the plate reader. The excitation wavelength used was 530 nm and the emission intensities were measured from 560 nm to 760 nm. Each sample was measured twice and the average maximum emissions at 610 nm used as a measure of the decrease in luminescence due to the displacement of the EthBr from the CT DNA by the complexes.

Apparent binding constants were calculated using the following equation:⁴³

Equation 4

$$K_{app} = \frac{K_e \times [\text{EthBr}]}{C_{50}}$$

where:

K_{app} = apparent binding constant.

$K_e = 9.5 \times 10^6 \text{ M}(\text{bp})^{-1}$.

C_{50} = concentration of complex required to reduce emission intensity at 610 nm by 50%.

Hairpin DNA

Luminescence with complexes 1 to 6³⁶

Stock solutions of all 10 hairpin DNA well-matched and mismatched base pairs in Tris buffer were prepared at a concentration of 6 μM . Stock solutions of the chloride salt of each complex were made up in Tris buffer at a concentration of 6 μM .

50 μL of each of the hairpin DNA solutions were added to wells in 10 vertical columns of a 96 well microplate. 50 μL of Tris buffer was added to the wells in the 11th column. 50 μL of each complex was then added to each well in a horizontal row so that the final concentrations in the wells were 3 μM for both the hairpin DNA and the complex. The plate was shielded from light and allowed to incubate at room temperature for one hour before the luminescence was analysed by plate reader. The excitation wavelength used was 450 nm and the emission intensities were measured from 550 nm to 800 nm.

The process was then repeated with a complex concentration in the well of 30 μM and, for complexes 1, 2 and 3, 1 μM and 0.3 μM . Each time the well concentration of the hairpin DNA was 3 μM .

12-Base oligonucleotide duplex DNA (12mers)

a) Luminescence with complexes 1 to 6³⁶

Stock solutions of the well-matched and CC mismatched 12mer DNA in Tris buffer were prepared at a concentration of 6 μM . Stock solutions of the chloride salt of each complex were made up in Tris buffer at concentrations of 6 μM and 60 μM .

Using a 96 well microplate, 50 μL of the well-matched and CC mismatched 12mer DNA solutions and 50 μL of the stock solutions of the complexes were mixed to achieve final well concentrations of 3 μM for the 12mer DNA and 3 μM and 30 μM for the complexes. Reference wells were set up consisting of the complexes only and 50 μL of Tris buffer. The plate was shielded from light and allowed to incubate at room temperature for one hour before being analysed using the plate reader. The excitation wavelength used was 450 nm and the emission intensities were measured from 550 nm to 800 nm.

Each complex was repeated twice at each concentration for both 12mer duplexes.

b) Luminescence via competitive displacement of ethidium bromide using complexes 1 to 8⁴³

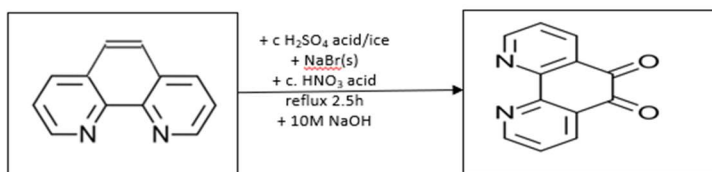
The method for the previous competitive displacement of EthBr from CT DNA was repeated using well concentrations for each DNA duplex (well-matched and CC mismatched) of 10 μM together with 3.5 μM EthBr. The complex concentrations in the wells were 1, 2.5, 5, 10, 25 and 50 (all μM) with the first row being reference wells containing Tris in lieu of the complexes. As before, the plate was shielded from light, incubated at room temperature for one hour and run at an excitation wavelength of 530 nm. The emission intensities were measured from 560 nm to 760 nm. Each condition was run twice and the average intensity at 610 nm used. Apparent binding constants were calculated using **Equation 4**.

3. Results and Discussion

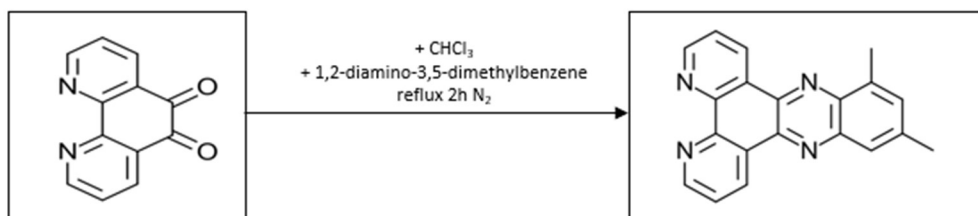
3.1 Syntheses

1,10-Phenanthroline-5,6-dione (phendione or dpq) was synthesized via **Scheme 1**. The 10,12-dimethyldipyridophenazine (dmdppz) ligand was prepared as shown by **Scheme 2**. Two synthetic pathways for the preparation of the target complexes were then attempted: a two step/direct route involving the addition of a pre-synthesised inserting functional group ligand (**Scheme 3**) and a three step method in which a $[\text{Ru}(\text{N}^{\wedge}\text{N})_2\text{dpq}](\text{PF}_6)_2$ intermediate is formed followed by a condensation reaction with a diamine (**Scheme 4**):

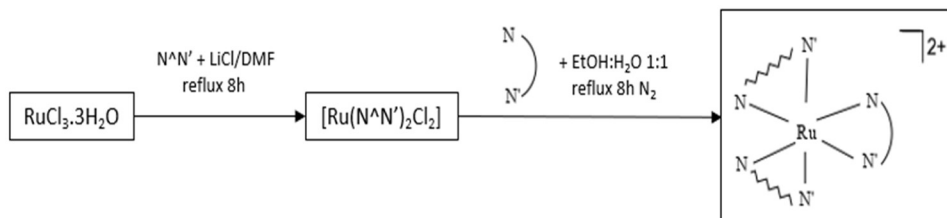
Scheme 1 – synthesis of 1,10-phenanthroline-5,6-dione (phendione or dpq)²⁸



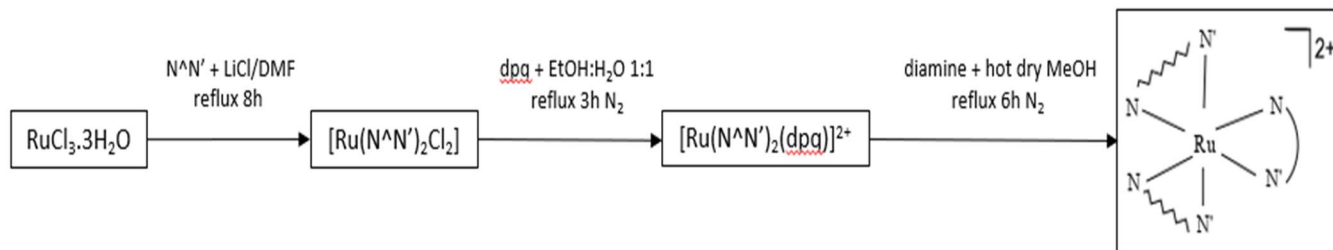
Scheme 2 – synthesis of 10,12-dimethyldipyridophenazine (dmdppz)²⁹



Scheme 3 – two step/direct route^{29,30}



Scheme 4 – three step method^{29,30}



Two step/direct route

The total reflux time for this method was 20.5 hours; it involved three recrystallisations, cooling at 4°C for 2x 16 hours and an overall oven drying time of 1 hour. The percentage yield for $\text{Ru}(\text{bpy})_2(\text{dmdppz})(\text{PF}_6)_2$ was 47 %.

Three step method

The total reflux time for this method was 19.5 hours; it involved two recrystallisations, cooling at 4°C for 16 hours and an overall oven drying time of 51 hours. The percentage yield for $[\text{Ru}(\text{bpy})_2(\text{dmdppz})](\text{PF}_6)_2$ was 70 %.

^1H NMR and mass spectrometry analysis confirmed the purity of the complexes prepared by both pathways. The log P value for the 12,17-dihydronaphthodipyridophenazine-12,17-dione or aqphen ligand, calculated using molinspiration, was 5.39.⁴⁴ This is high relative to that for the 10,12-dimethyldipyridophenazine or dmdppz ligand (4.51) and it was felt that this level of hydrophobicity was likely to prove problematic when coordinating the aqphen ligand directly to the $[\text{Ru}(\text{N}^{\wedge}\text{N})_2\text{Cl}_2]$ in ethanol:water 1:1.⁴⁴

Based on the larger percentage yield, the slightly more facile experimental details and the potential issues associated with hydrophobicity, it was decided to use the two step method with the phendione/dpq already co-ordinated to the Ru(II) before condensation with the diamine for all the other complexes.

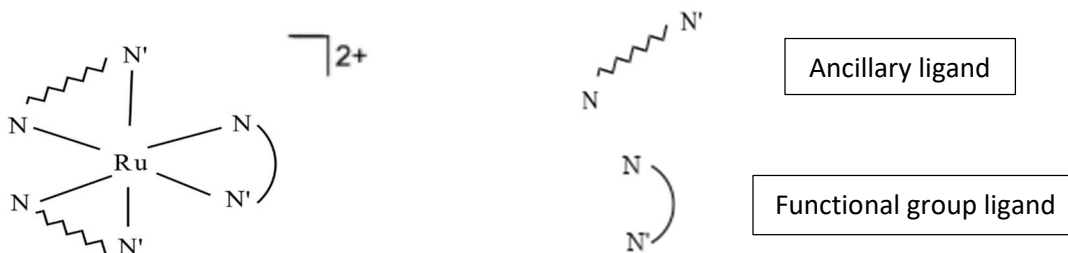
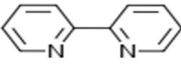
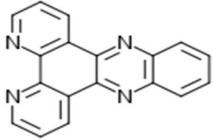
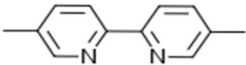
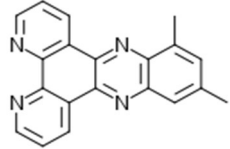
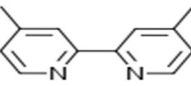
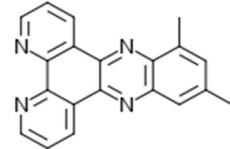
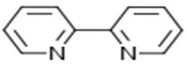
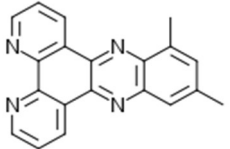
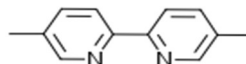
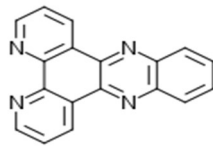
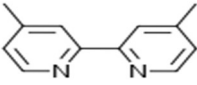
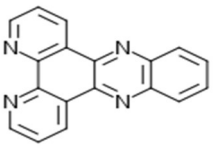
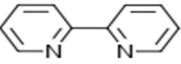
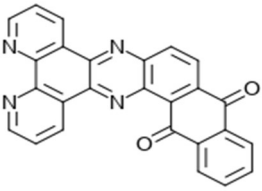
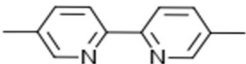
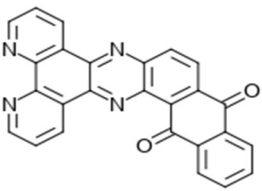


Fig. 30 Octahedral polypyridyl ruthenium (II) complexes.

Table 4. Complexes synthesized including ancillary ligands.

	Novel	Yield %		Ancillary ligand	Functional group ligand
1	No	35	$[\text{Ru}(\text{bpy})_2(\text{dppz})](\text{PF}_6)_2$		
2	Yes	87	$[\text{Ru}(5,5'\text{-dmbpy})_2(\text{dmdppz})](\text{PF}_6)_2$		
3	Yes	81	$[\text{Ru}(4,4'\text{-dmbpy})_2(\text{dmdppz})](\text{PF}_6)_2$		
4	Yes	70	$[\text{Ru}(\text{bpy})_2(\text{dmdppz})](\text{PF}_6)_2$		
5	No	82	$[\text{Ru}(5,5'\text{-dmbpy})_2(\text{dppz})](\text{PF}_6)_2$		
6	Yes	66	$\text{Ru}(4,4'\text{-dmbpy})_2(\text{dppz})](\text{PF}_6)_2$		
7	No	88	$[\text{Ru}(\text{bpy})_2(\text{aqphen})](\text{PF}_6)_2$		
8	Yes	66	$[\text{Ru}(5,5'\text{-dmbpy})_2(\text{aqphen})](\text{PF}_6)_2$		

3.2 UV/VIS absorption spectra

UV/VIS absorption spectra of the eight ruthenium complexes were measured to confirm the metal-to-ligand charge-transfer (MLCT) peaks at approximately 450 nm as well as the higher energy ligand-centred transitions. The absorbances at 450 nm were used to calculate the Luminescence Quantum Yields.

Table 5. Wavelengths λ_{\max} and molar extinction coefficients ϵ for selected absorbances of complexes in acetonitrile.

Complex	Band A		Band B		Band C	
	λ_{\max} [nm]	ϵ [dm ³ mol ⁻¹ cm ⁻¹]	λ_{\max} [nm]	ϵ [dm ³ mol ⁻¹ cm ⁻¹]	λ_{\max} [nm]	ϵ [dm ³ mol ⁻¹ cm ⁻¹]
1	284	2.03E+05	364	3.24E+04	449	3.03E+04
2	293	1.05E+05	372	1.54E+04	436	1.61E+04
3	289	9.65E+04	371	1.84E+04	454	1.57E+04
4	288	8.01E+04	370	1.23E+04	454	1.25E+04
5	290	9.28E+04	367	1.67E+04	435	1.62E+04
6	283	1.16E+05	360	2.38E+04	446	1.93E+04
7	286	6.48E+04	397	1.13E+04	442	1.06E+04
8	291	5.79E+04	395	1.09E+04	440	9.22E+03

For complexes 7 and 8, the increased delocalization on the aqphen compared to the dmdppz and the dppz functional group ligands makes the aromatic system more stable reducing the energy gap to the antibonding π^* molecular orbital. This makes λ_{\max} in Band B longer and means that it merges into λ_{\max} for Band C, the MLCT absorbance, for both these complexes. This is shown in **Fig. 31** for complex 8 in comparison to complexes 2 and 5:

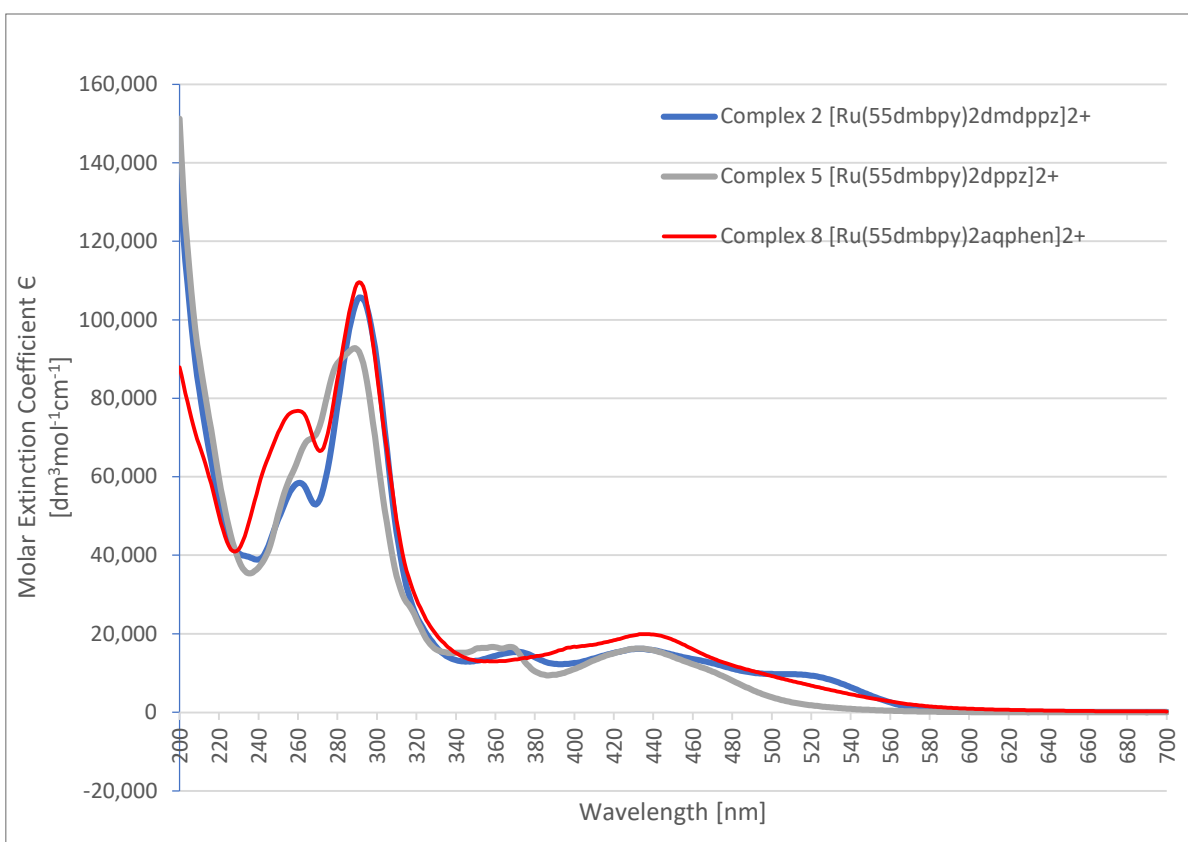


Fig. 31 UV/VIS absorption spectra for complexes 2, 5 and 8 in acetonitrile.

3.3 Luminescence excitation and emission spectra

Luminescence emission spectra were measured to investigate the variation in the wavelength of the emission maxima and to find out the integrated emission intensities to calculate the Luminescence Quantum Yields. Excitation spectra were measured to find out all the excitation wavelengths which would cause the emission maxima.

Table 6. Wavelengths of maxima in excitation and emission spectra and emission intensities for complexes in acetonitrile. AU = arbitrary units.

Complex	λ_{\max} for excitations in nm	λ_{\max} for emission in nm	Emission intensity of λ_{\max} in AU	Emission intensity of λ_{\max} relative to complex 1
1	303, 367, 448	610	0.912	1.000
2	303, 370, 440	612	0.362	0.397
3	310, 370, 449	619	0.641	0.703
4	298, 367, 445	601	0.489	0.536
5	306, 364, 436	618	0.166	0.182
6	311, 359 - broad, 452	625	0.237	0.260
7	297, 454 - broad	600	0.044	0.048
8	298	604	0.109	0.120

For emission spectra from 500-750nm the excitation wavelength used was 450nm (**Fig. 32**). For complexes 5 and 6 (with methylated bpy ancillary ligands only) there is a small red shift for the emission compared to complex 1. The same is true for complexes 2 and 3 in which the dppz functional group ligand is methylated as well although for complex 2 the red shift is very slight. Interestingly, for complex 4 in which only the dppz functional group ligand is methylated there is a small blue shift compared to complex 1. The highest emission intensity recorded was for complex 1 with the lowest for complexes 7 and 8. Complex 7 is practically non-emissive which is consistent with previous work employing the aqphen ligand.^{16,31}

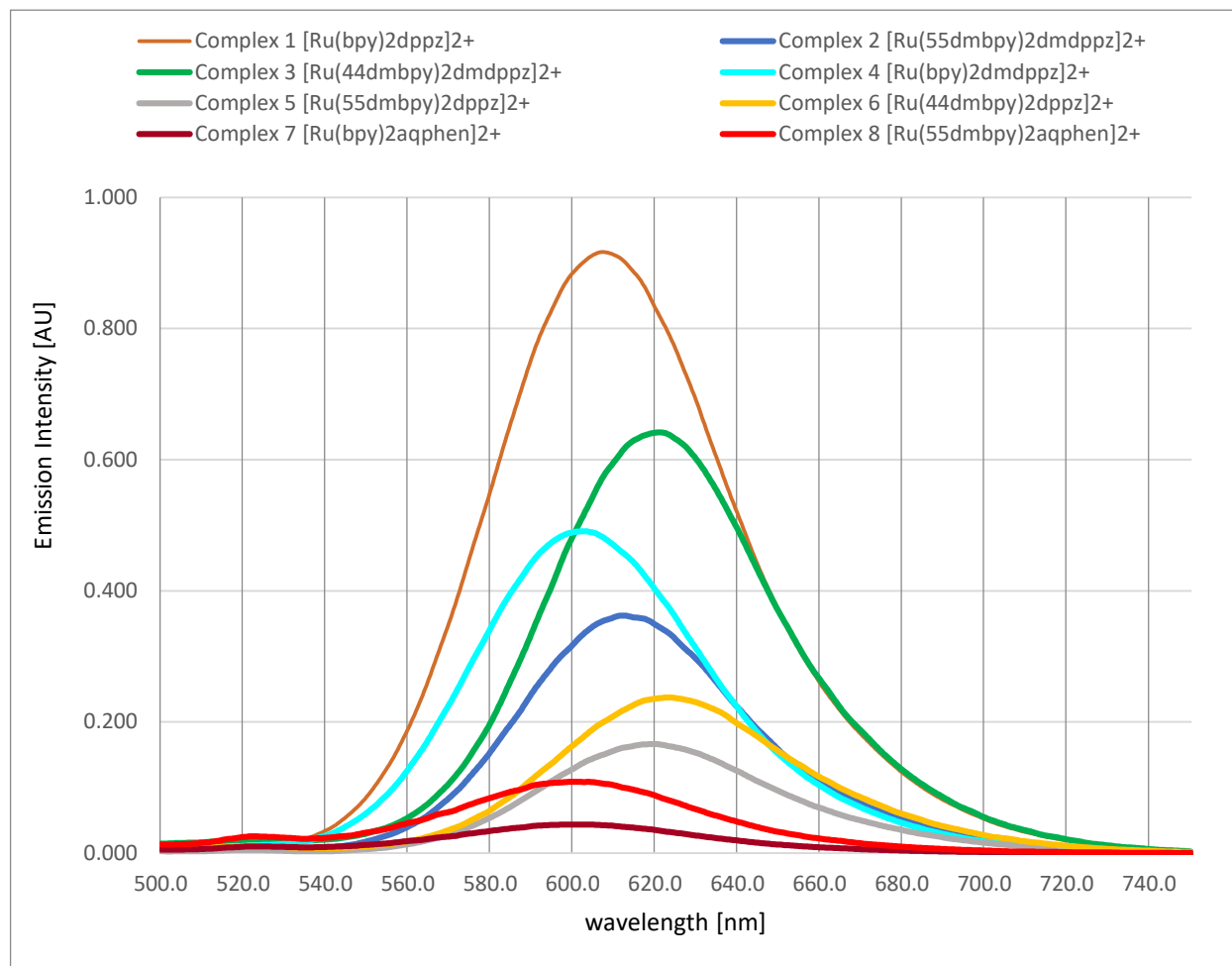


Fig. 32 Emission spectra for all complexes in acetonitrile. Excitation wavelength = 450 nm.

Excitation spectra (**Fig. 33**) were measured from 280-500nm with the emission wavelength set between 600-623nm depending upon the maximum peak intensity observed in each emission spectrum. In all cases the distinctive second order harmonic at half the emission wavelength is clearly visible in the excitation spectra.

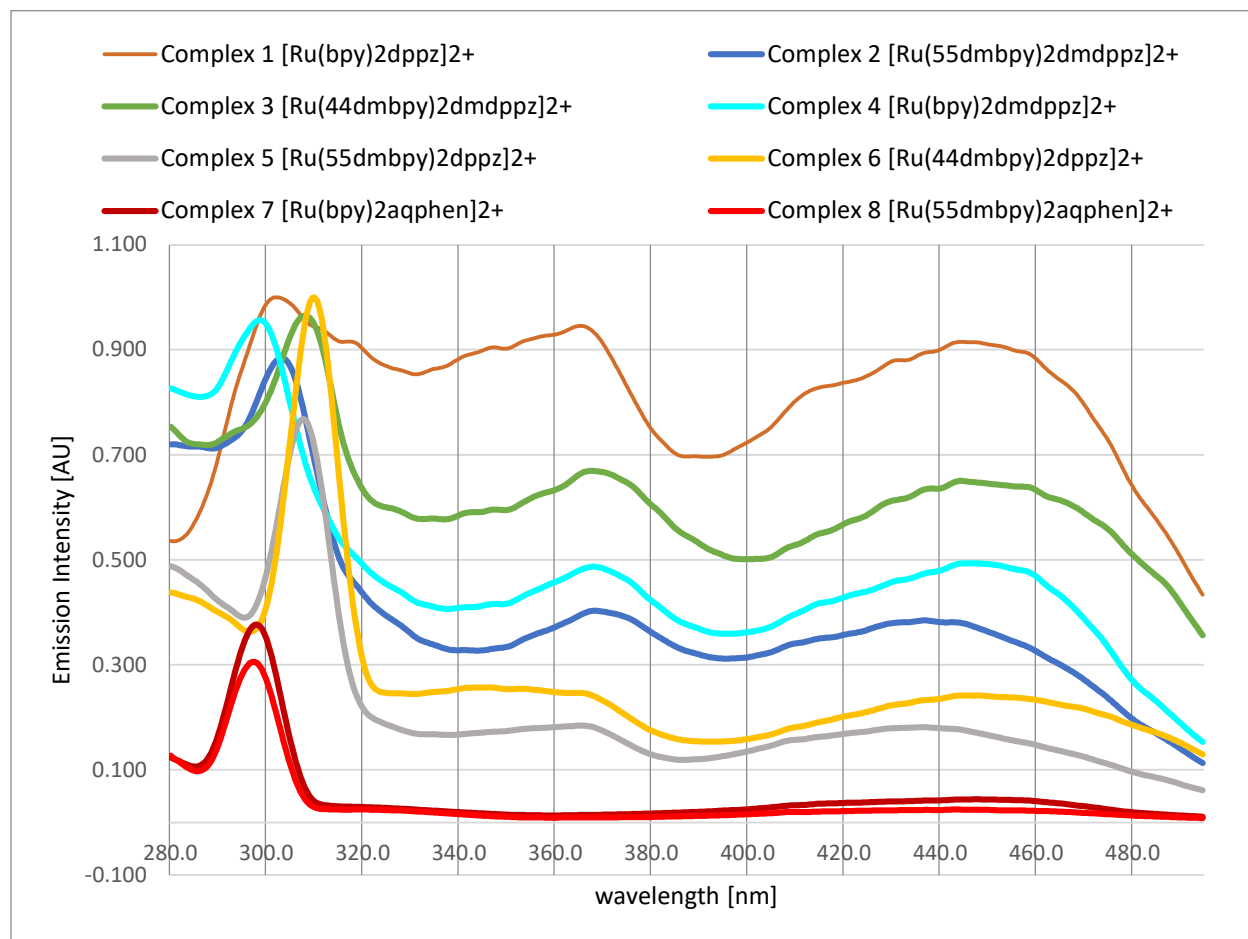


Fig. 33 Excitation spectra for all complexes in acetonitrile.

The complexes obey the mirror-image rule for their absorption and emission spectra as illustrated by complex 4 (**Fig. 34**) in that the MLCT absorption peak 450nm is mirrored by the emission at 600nm (the higher energy absorption peaks are ligand-centred). The peaks in the excitation spectra also correspond well to those in the absorption spectra indicating that the luminescence is due to transition from the lowest energy triplet $^3\text{MLCT}$ excited state.¹³

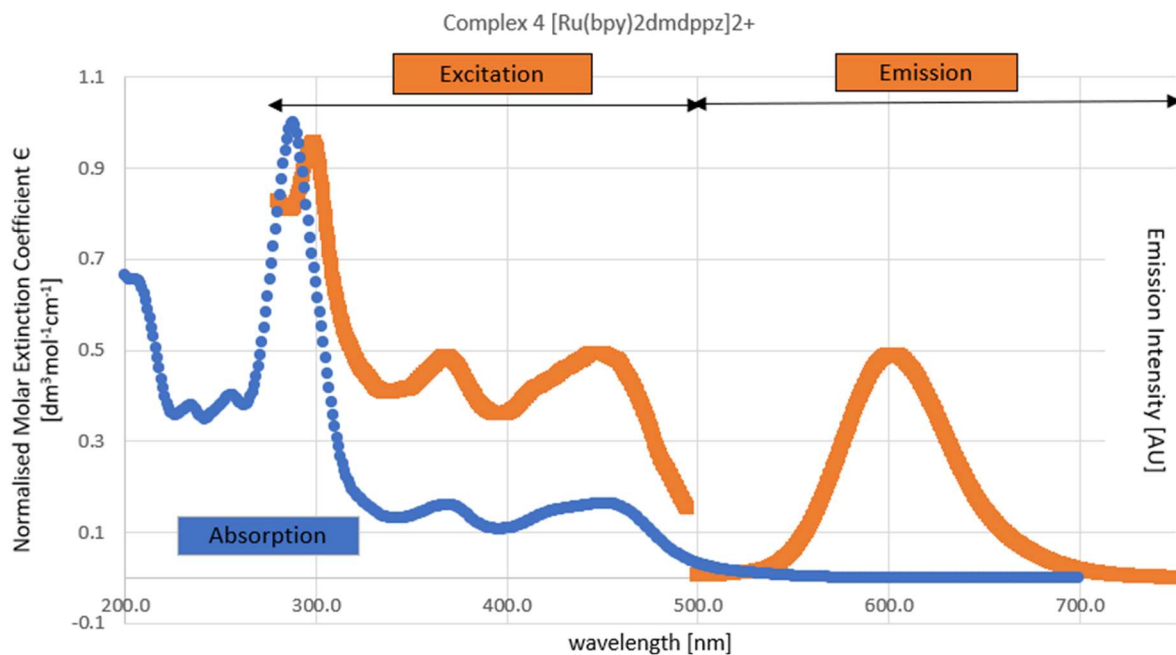


Fig. 34 Electronic absorption, excitation and emission spectra for complex 4 in acetonitrile.

3.4 Luminescence Quantum Yields Q at $\lambda_{\text{ex}} = 450\text{nm}$

Luminescence Quantum Yield or Efficiency Q is the ratio of the number of photons emitted during luminescence to the number of photons absorbed by a fluorophore during excitation. It was calculated for all 8 complexes using **Equations 1 and 2** using $[\text{Ru}(\text{bpy})_3]^{2+}$ as the reference:

$$Q_r = 0.018 \pm 0.002 \text{ at } \lambda_{\text{ex}} = 450\text{nm in acetonitrile.}^{33}$$

$$Q_r = 0.040 \pm 0.002 \text{ at } \lambda_{\text{ex}} = 450\text{nm in water.}^{33}$$

Table 7. Luminescence Quantum Yields Q of complexes.

Complex	Quantum Yield Q_{MeCN}	$Q_{\text{MeCN}}/Q_{\text{MeCN complex 1}}$	Quantum Yield Q_{H2O}
1	0.0081 ± 0.001	1.0	
2	0.012 ± 0.001	1.5	
3	0.012 ± 0.001	1.5	
4	0.016 ± 0.002	2.0	
5	0.011 ± 0.001	1.4	
6	0.0082 ± 0.001	1.0	
7	0.0013 ± 0.00015	0.2	0.0033 ± 0.0002
8	0.00030 ± 0.00003	0.04	0.00058 ± 0.00003
$[\text{Ru}(\text{bpy})_3]^{2+}$	0.018 ± 0.002	2.2	0.040 ± 0.002

The data confirm that Complexes 7 and 8 are weakly emissive, although their quantum yields are higher in DI water. Methylation of the dppz ligand leads to a doubling of the quantum yield for complex 4 compared to complex 1. Substantial increases have been reported previously for $[\text{Ru}(\text{phen})_210\text{-methyl dppz}]^{2+}$ when bound to DNA.⁴⁵ However, **Table 7** shows that quantum yield is decreased when the bpy ancillary ligands are methylated as well, comparing complexes 2 and 3 to complex 4. This is in contrast to what is observed for the unmethylated dppz complexes 5 and 6, where a greater or equal quantum yield is seen for the methylated bpy ancillary ligand derivatives compared to complex 1. Hager and Crosby⁴⁶ reported a decrease in the quantum yield from $[\text{Ru}(\text{bpy})_3]^{2+}$ to $[\text{Ru}(4,4'\text{-dmbpy})_3]^{2+}$ which means that the trend for the unmethylated dppz in this study is the unexpected one.

3.5 DNA binding studies

3.5.1 CT DNA

a) Luminescence titrations with complexes 1 to 6

Luminescence spectra in Tris buffer were collected (**Fig. 35**) and curves of fraction of complex bound to DNA versus $[DNA]/[complex]$ (**Fig. 36**) plotted to generate Scatchard plots (**Fig. 37**).

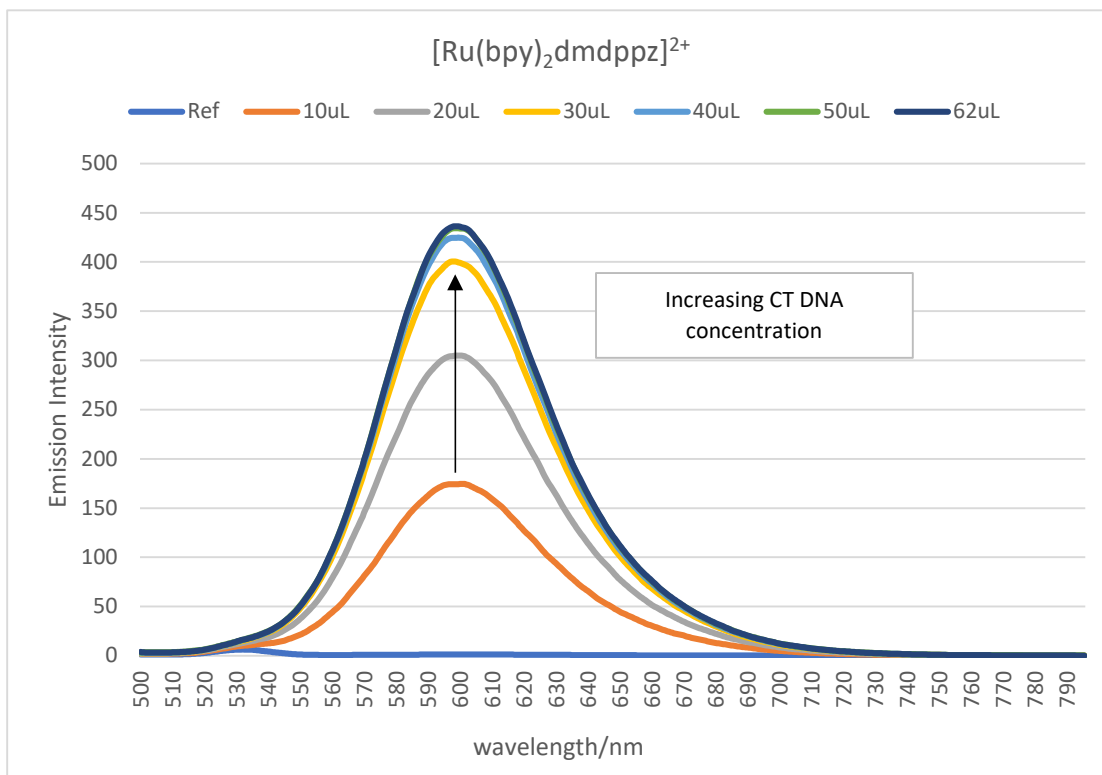


Fig. 35 Changes in luminescence emission spectrum of complex 4 $[Ru(bpy)_2dmdppz]^{2+} = 3 \mu M$ in Tris buffer on addition of CT DNA.

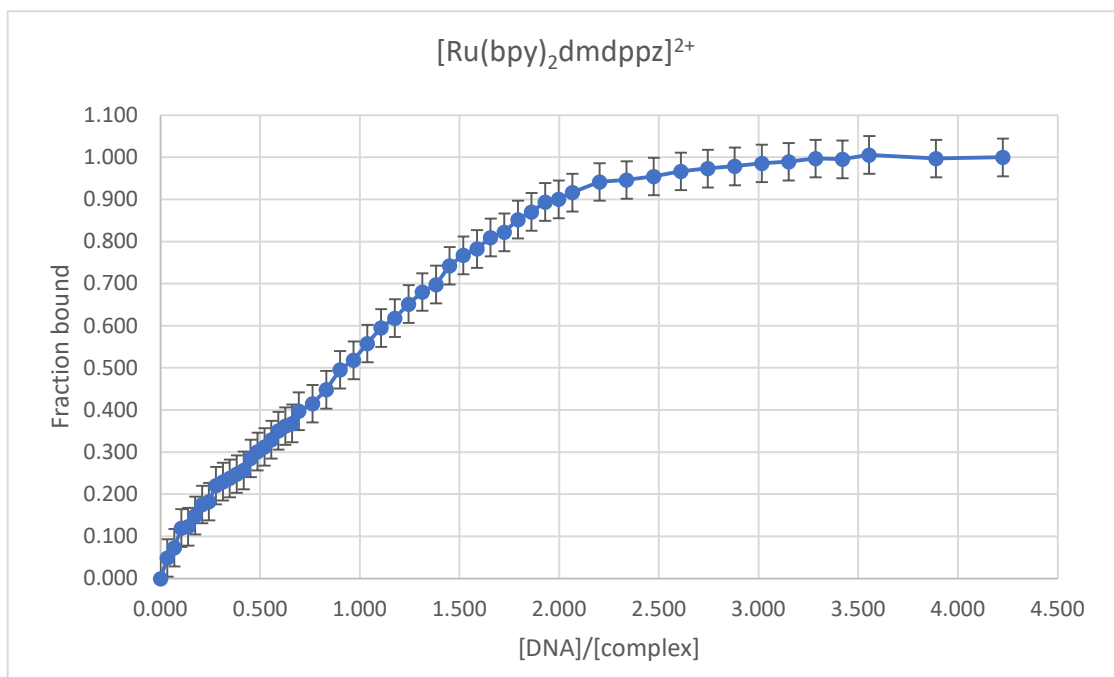


Fig. 36 Plot of fraction of complex 4 bound to CT DNA (measured via maximum emission intensity) vs $[DNA]/[complex]$.

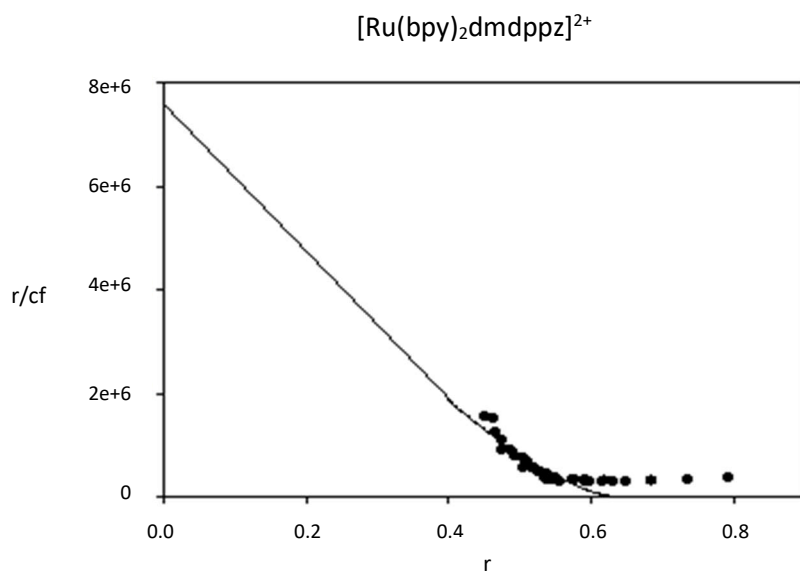


Fig. 37 Scatchard plot r/cf vs r for complex 4. r = number of moles of complex 4 bound per mole of nucleotide (measured via maximum emission intensity). cf = concentration of unbound complex 4.⁴⁷

Values for binding constants K_b , and site sizes (number of base pairs per site) n were calculated by fitting the Scatchard plots to the McGhee-von Hippel equation.⁴⁰ The fraction bound was measured using the area under the curve (AUC) as well as the maximum emission intensity (max ei) for comparative purposes (**Table 8**). The titrations were carried out in PBS buffer by way of further comparison.

Table 8. Binding constants and site sizes for complexes in Tris buffer via luminescence
(a) AUC yellow (b) max ei blue.

Complex	Coefficient of determination R^2	Binding constant K_b	Site size (no. of base pairs per site) n	$K_b/K_b_{\text{complex 1}}$
1	0.8917	2.513E+06	1.2625	1.00
	0.8840	1.545E+06	1.1330	1.00
2	0.9273	9.225E+06	1.3945	3.67
	0.9270	9.663E+06	1.3970	6.26
3	0.9245	5.650E+06	0.7083	2.25
	0.8370	5.505E+06	0.6920	3.56
4	0.8843	8.711E+06	1.6031	3.47
	0.8160	7.549E+06	1.5710	4.89
5	0.9373	2.632E+06	1.7270	1.05
	0.8780	1.902E+06	1.4960	1.23
6*	0.8520	2.539E+06	0.5404	1.01
	0.8150	2.744E+06	0.5550	1.78

*Based on the reduced number of data points fitted, it appears that the McGhee-von Hippel equation⁴⁰ has not worked for complex 6 in which the ancillary ligands only are methylated at positions 4,4'. Therefore, values of K_b and n could not be determined with reliability for this complex which means that comparisons of binding affinities could not be made with any degree of confidence.

If the values for complex 6 are discarded then the same order of binding strength ($2 > 1 > 3 > 5 > 4$) is observed for the other complexes using both the max ei and the AUC methods. Therefore, it can be concluded that using max ei is a suitable alternative to the use of AUC for the measurement of the fraction of the complex bound to DNA, although it should be noted that the actual values of the binding constants calculated are slightly higher via the latter approach (complex 2 is the exception to this pattern). Max ei was used for all further luminescence work.

For complex 3 in PBS buffer, a much lower binding affinity was recorded ($8.59E+05$) and only 11 data points could be fitted; similar problems in terms of the number of data points that could be fitted were found with the other complexes in PBS and all further DNA binding studies were carried out in Tris buffer as a consequence.

Table 9. Luminescence Quantum Yield, binding constant and maximum luminescence ratios for complexes.

Complex	Quantum Yield $Q_{\text{MeCN}}/Q_{\text{MeCN}}$ complex 1	Binding constant K_b/K_b complex 1	Luminescence $I_{\text{max}}/I_{\text{max}}$ complex1
1	1.0	1.0	1.0
2	1.5	6.3	3.5
3	1.5	3.6	4.4
4	2.0	4.9	8.7
5	1.4	1.2	0.4
6*	1.0	1.8	0.6

Summarising the Quantum Yield, luminescence titration and binding constant results (**Table 9**), it can be seen that methylation of the dppz functional group ligand at positions 10 and 12 has resulted in a greater affinity for DNA, where all three dmdppz complexes have a larger K_b value than their corresponding dppz complex. The binding constant for complex 2 is the highest of the six complexes. All three dmdppz complexes demonstrate a large increase in luminescence compared to complex 1 which can be attributed to the higher quantum yields coupled with the stronger binding affinities. Interestingly, although complexes 2 and 3 have the same quantum yields, complex 3 with the methylation of the ancillary ligands in the 4,4' position has a higher luminescence but a lower binding affinity than complex 2 with the methylation at the 5,5' position.

Methylation of the ancillary ligands only in complex 5 lowers the luminescence compared to complex 1, although the binding is stronger and the quantum yield is higher. The decrease in luminescence caused by methylation on the bpy ligands is consistent with the values observed for complexes 2 and 3 compared to complex 4. It seems, therefore, that increasing the steric bulk of the ancillary ligands in this way retains more quenching of the signal due to hydrogen bonding of the phenazine N atoms with water.

b) UV/VIS titrations with complexes 1, 7 and 8

Complexes 7 and 8, which both contain the aqphen functional group ligand, are weakly emissive in both aprotic and protic solvents due to the intramolecular photoinduced electron transfer (PET) effect of the quinone moiety which quenches the $^3\text{MLCT}$ emission. This means that they do not exhibit "light switch" behaviour and so their interaction with DNA was investigated by measuring the hypochromicity in their UV/VIS spectra with increasing amounts of DNA (**Fig. 38**).

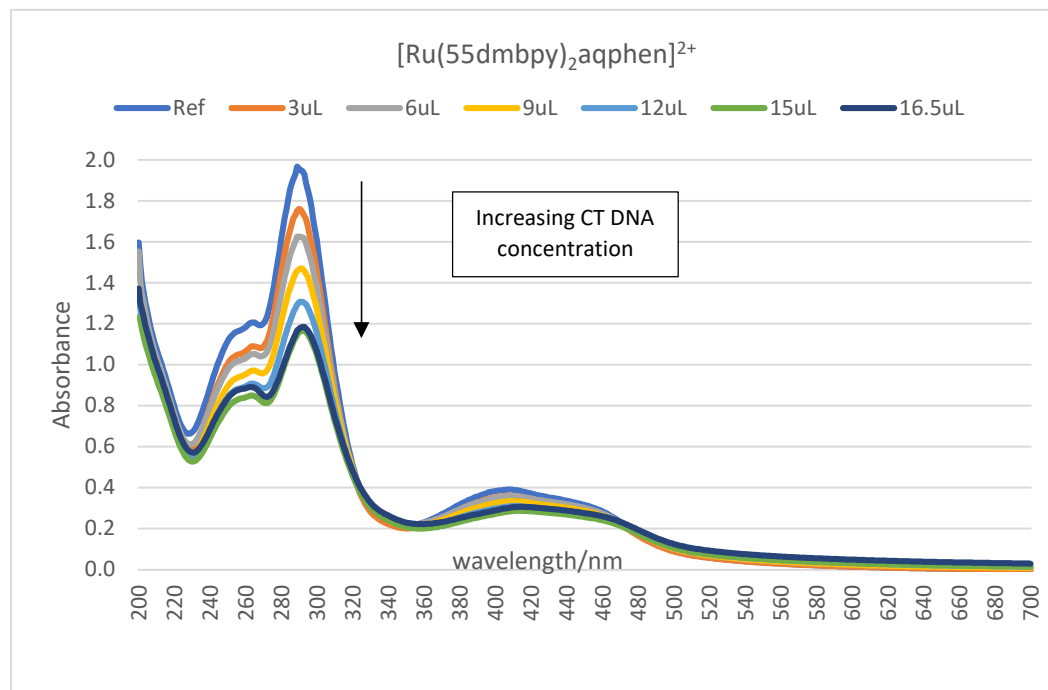


Fig. 38 Changes in UV/VIS absorption spectrum of complex 8 $[\text{Ru}(5,5'\text{-dmbpy})_2\text{aqphen}]^{2+} = 30 \mu\text{M}$ in Tris buffer on addition of CT DNA.

As before, curves of fraction of complex bound to DNA versus $[\text{DNA}]/[\text{complex}]$ were used to generate Scatchard plots from which values for binding constants K_b and site sizes (number of base pairs per site) n were calculated. The fraction of the complex bound was measured using the decrease in absorbance at approximately 290nm.

Table 10. Binding constants and site sizes for complexes 4, 7 and 8 in Tris buffer via UV/VIS absorption.

Complex	Coefficient of determination R^2	Binding constant K_b	Site size (no. of base pairs per site) n	$K_b/K_b_{\text{complex 1}}$
1	0.8166	7.373E+05	1.5247	1.00
7	0.9049	1.607E+06	0.5747	2.18
8	0.8714	1.661E+06	0.5556	2.25

Complex 1 was included to enable comparison of the binding constants with those obtained from the luminescence titrations. The lower binding constant recorded for complex 1 via UV/VIS absorption could be a consequence of the different technique used. Nevertheless, it can be concluded that complexes 7 and 8 with the aqphen functional group ligands are higher affinity binders for DNA than complex 1, with the methylated bpy ancillary ligands in complex 8 raising the binding strength further.

c) Luminescence via competitive displacement of ethidium bromide using complexes 1, 5, 7 and 8

To investigate further the effect of the technique used on the binding constants obtained for the weakly emissive aqphen complexes, apparent binding constants K_{app} were measured using a displacement assay involving ethidium bromide EthBr, a fluorophore and classic DNA intercalator (**Fig. 39**).^{48,49} CT DNA was first loaded with EthBr and the consequent quenching of EthBr luminescence due to the competitive displacement by the ruthenium complex employed to examine binding.

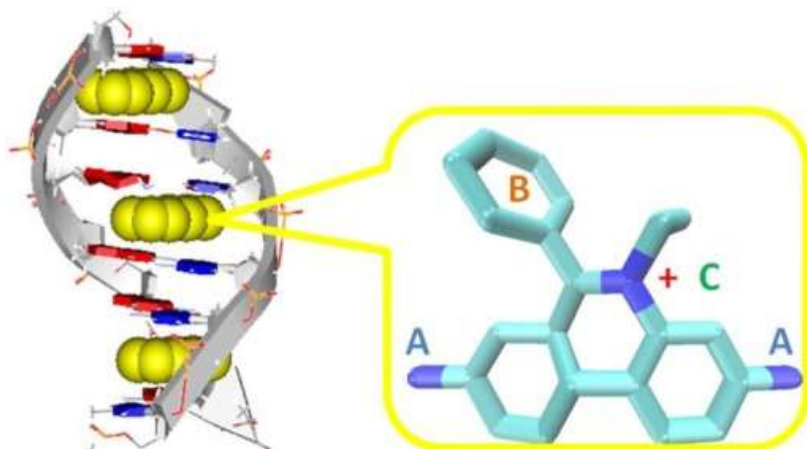


Fig. 39 Model of crystal structure of ethidium bromide with DNA showing the intercalative binding mode: A) amino substituents responsible for luminescence increase upon DNA intercalation; B) phenyl substituent for steric control and also impact on fluorimetric properties; C) permanent positive charge for aqueous solubility and electrostatic attraction to the DNA phosphate backbone.⁴⁹

Complex 1 was the term of comparison . Complex 5 was included as it had led to the greatest reduction in the signal in the luminescence titrations and had the lowest binding constant compared to complex 1. It was thought, therefore, that it would provide the biggest contrast to the aqphen complexes.

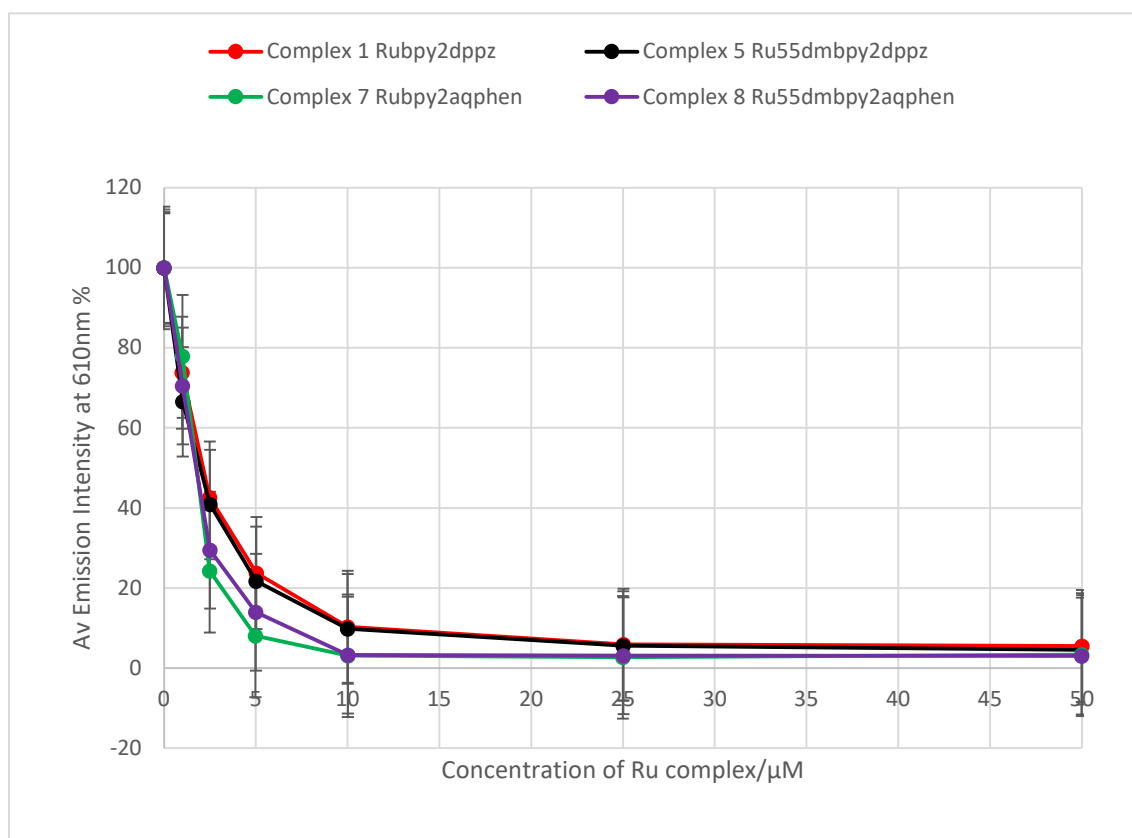


Fig. 40 EthBr displacement assays with CT DNA: plots of average emission intensities at 610nm vs [Ru complexes] in Tris buffer for complexes 1, 5, 7 and 8. Excitation wavelength = 530nm.

The concentration of each complex needed to reduce the EthBr emission intensity by 50%, C_{50} , was determined from the graphs in **Fig. 40** and values for apparent binding constants K_{app} calculated from **Equation 4**.

Table 11. Apparent binding constants for complexes 1, 5, 7 and 8 in Tris buffer via EthBr displacement assay.

Complex	Concentration of complex to reduce emission intensity by 50% C_{50}	Apparent binding constant K_{app}	$K_{app}/K_{app \text{ complex 1}}$
1	2.13	1.61E+07	1.00
5	1.98	1.73E+07	1.07
7	1.78	1.93E+07	1.20
8	1.76	1.95E+07	1.21

From these derived apparent binding constants, the overall order of DNA binding affinity is: 8>7>5>4. The binding constants for complexes 1 and 5 are approximately 10x higher than those calculated from the luminescence titrations which, for complex 1, was double that obtained via UV/VIS absorption. It appears, therefore, that the technique used does make a difference to the actual value of the binding constant calculated. However, the order of binding strength from the EthBr displacement assay is in agreement with the UV/VIS results, where an order of DNA binding affinity 8>7>1 was observed, and also with the luminescence titrations which indicated that complex 5 binds more strongly than complex 1.

3.5.2 Hairpin DNA

To look at the mismatch selectivity of the Ru complexes synthesized, hairpin or hairpin loop DNA was used. This type of DNA occurs when two regions of the same strand base-pair to form a double helix that ends in an unpaired loop. In this study the DNA employed consisted of a loop of five Thymine bases with 12 base pairs; the base pairs were either all well-matched or one of them was mismatched (**Table 2**).

Table 2. Hairpin DNA sequences.

T	T	T	C	G	G	T	A	X	G	G	A	C	G	G	5'
T	T	T	G	C	C	A	T	Y	C	C	T	G	C	C	3'

X	G	A	A	C	G	T	A	C	C	G
Y	C	T	A	C	G	T	G	A	T	T
well-matched			mismatched							

Luminescence with complexes 1 to 6

Consistent with the CT DNA luminescence titrations, complexes 2, 3 and 4 all demonstrated increased emission intensity compared to complex 1 upon the addition of each DNA hairpin, with complex 4 showing the greatest signal. Methylation of the bpy ancillary ligands only in complexes 5 and 6 reduced the signal below that of complex 1 which, once more, is consistent with the CT DNA work but the different well-matched and mismatched base pairs show maxima at different intensities (**Figs. 41, 42 and 43**). In **Fig. 42** for complex 5 it can be seen that the maximum signals for the CC and TT mismatch-containing hairpins have a three-fold increase in intensity compared to the peaks for the other hairpins. This is not the case for complex 6 in **Fig. 43** in which all the peaks have a similar intensity. This appears to indicate that methylation specifically at the 5,5' position on the bpy ancillary ligands is leading to selective and strong signals for these mismatches.

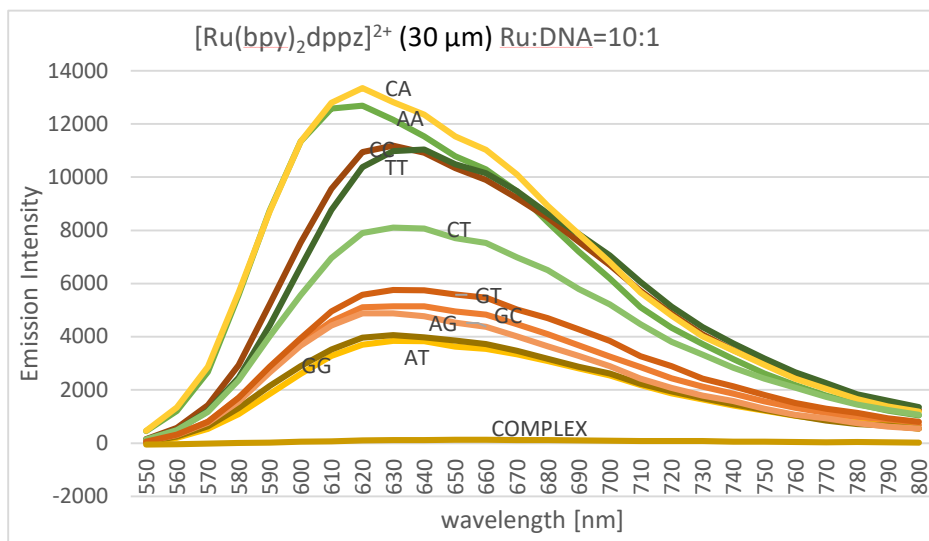


Fig. 41 Luminescence emission spectrum of complex 1 [Ru(bpy)₂dppz]²⁺ = 30 μm in Tris buffer on addition of DNA hairpins.

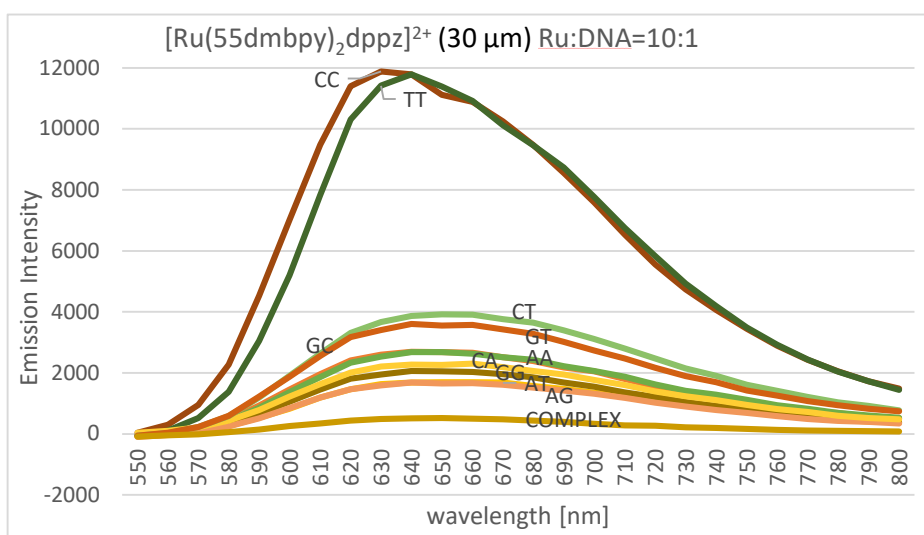


Fig. 42 Luminescence emission spectrum of complex 5 [Ru(55dmbpy)₂dppz]²⁺ = 30 μm in Tris buffer on addition of DNA hairpins.

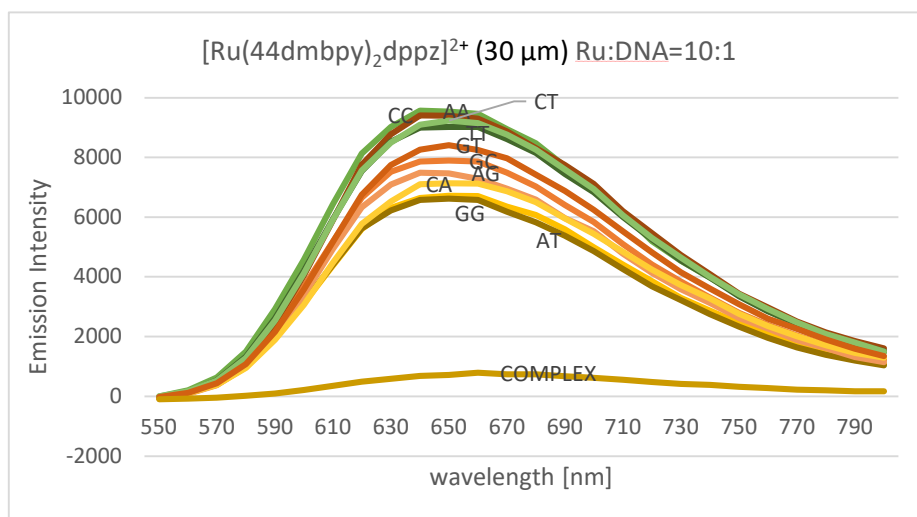
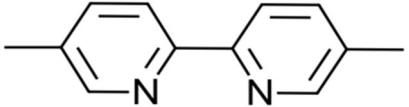
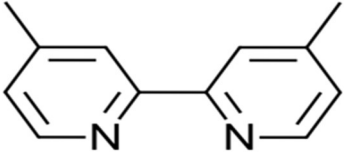


Fig. 43 Luminescence emission spectrum of complex 6 $[\text{Ru}(44\text{dmbpy})_2\text{dppz}]^{2+} = 30 \mu\text{m}$ in Tris buffer on addition of DNA hairpins.

Figs. 42 and 43 show that when the ancillary bpy ligands are methylated in the 5,5' positions as opposed to the 4,4' positions the maximum emission intensities recorded are lower except for the CC and TT mismatches. To explain this it is useful to consider the projection radii of the respective ligands.

Table 12. Projection radii and maximum diameters of methylated bpy ligands on complexes 5 and 6.⁵⁰

	
5,5'-dimethyl-2,2'-bipyridine	4,4'-dimethyl-2,2'-bipyridine
projection radius = 6.65Å	projection radius = 6.23Å
maximum diameter of ligand = 13.30Å	maximum diameter of ligand = 12.46Å
Complex 5 $[\text{Ru}(5,5'\text{dmbpy})_2\text{dppz}]^{2+}$	Complex 6 $[\text{Ru}(4,4'\text{dmbpy})_2\text{dppz}]^{2+}$

The presence of increased steric bulk due to the protruding substituent methyl groups on the ancillary bpy ligands could prevent deep intercalation of the inserting dppz functional group ligand into the base stack of DNA^{12,51} thus retaining significant quenching by water and a lower signal. Having the methyl groups in the 5,5' positions means a larger projection radius than in the 4,4' positions, which means that the former is more effective at reducing intercalation and will produce a lower signal again than the latter. However, this still leaves the question as to why the intensities for complex 5 with the CC and TT mismatch base pairs are so high?

To look at the selectivity of all the complexes when bound to the different well-matched and mismatched base pairs in hairpin DNA in more detail, the data was presented as a series of bar charts (**Fig. 44**). The largest differences were observed with [Ru complex]:[DNA] = 10:1 and the height of each bar was calculated from the area under the curve for each base pair normalized to the well-matched AT pairing using OriginLab software.⁵²

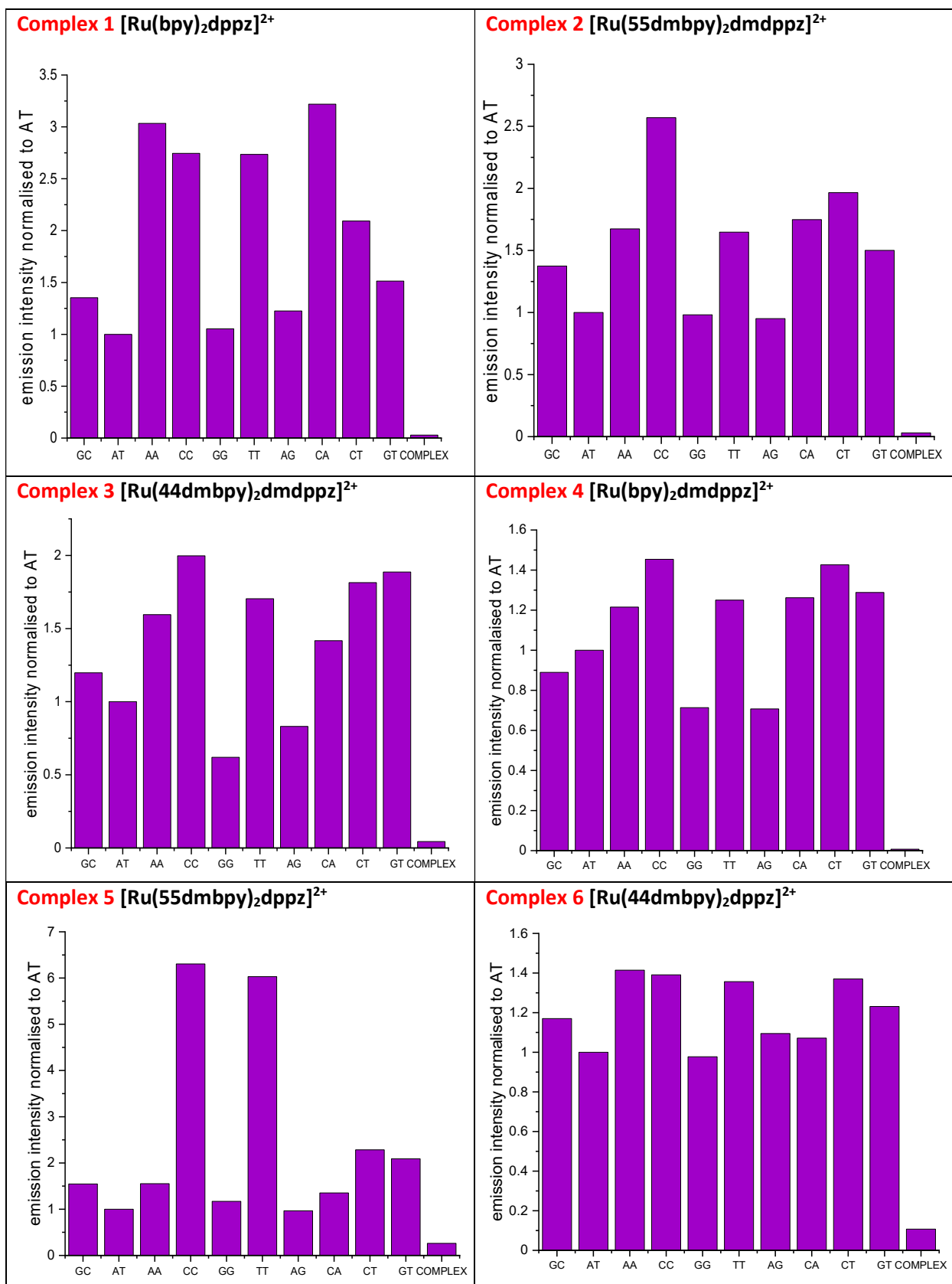


Fig. 44 Emission intensities for complexes 1 to 6 with DNA hairpins in Tris buffer. All [Ru complexes] = 30.0 μ M and signals normalized to AT base pair. [DNA hairpins] = 3 μ M.

On the basis of these data, all complexes display selectivity for the CC mismatch with complex 5 showing the highest degree of selectivity for the hairpin containing this mismatch. Complex 5 also shows a large increase in emission for the TT mismatch and this is mirrored by the other complexes, although not to the same magnitude.

Although the selectivity for the CC and TT mismatches is significant, all the complexes also show some selectivity towards the AA, CA, CT and GT mismatches. In addition, the signal for the GG mismatch is either lower or approximately equal to that for the well-matched AT base pair across all six complexes. The AG mismatch is less predictable in that its signal is lower than AT for complexes 1 and 3, the same for complexes 2 and 5 but higher for complexes 4 and 6. This compares favourably to previous photocleavage data for Δ -[Rh(bpy)₂(chrysi)]³⁺ (**Fig. 2**) which observed the strongest cleavage at CC, CA and CT sites, intermediate cleavage at TT sites and much smaller cleavage at GG and AG sites.⁵³ Thermodynamic data derived⁵³ from the same study gave the following order of thermodynamic stability: CC>TT>CT>CA>AA.

One explanation as to why the emission intensities for CC and TT are so high is, therefore, because they are the least thermodynamically stable of the mismatch base pairs. This would mean they are likely to bind most strongly to the complexes thus reducing the quenching due to water to the largest extent and producing the greatest signals.

Interestingly at lower complex concentrations the differences between the well-matched and mismatched base pairs were much smaller (**Fig. 45**). This could be explained by the presence of a large excess of binding sites on the DNA: either 11 well-matched and one mismatched or 12 well-matched for each hairpin. This would mean that the ruthenium complexes bind at random and so any signal differences due to the different binding sites used would be a matter of chance. As the concentration of the complex increases, a greater number of binding sites would be occupied and, if a best fit in terms of stability were to apply, signal differences between the XY base pairs in the hairpins would emerge.

Complex 2 [Ru(55dmbpy)₂dmdppz]²⁺

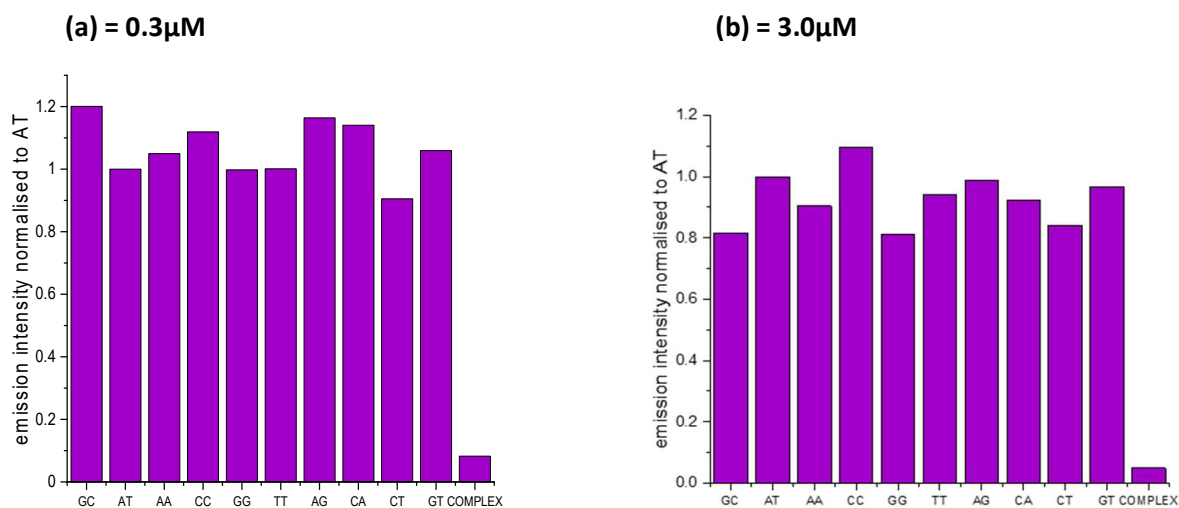


Fig. 45 Emission intensities for complex 2 with DNA hairpins in Tris buffer. [Ru complex] = (a) 0.3 μM and (b) 3.0 μM. Signals normalized to AT base pair. [DNA hairpins] = 3 μM

3.5.3 12-Base oligonucleotide duplex DNA (12mers)

To investigate CC mismatch selectivity further, duplex DNA was prepared from 12 nucleotide sequences such that the base pairing was the same as the hairpin DNA but without the five Thymine base loop. Two 12mer duplexes were used: one in which all the base pairs were well-matched and the other containing a single CC mismatch (**Table 3**).

Table 3. 12mer DNA sequences.

3'	C	G	G	T	A	X	G	G	A	C	G	G	5'
5'	G	C	C	A	T	Y	C	C	T	G	C	C	3'

X	G	C
Y	C	C
	well-matched	mismatched

a) Luminescence with complexes 1 to 6

Table 13. Maximum emission intensities for complexes 1 to 6 with 12mers in Tris buffer at [Ru complexes] = 3.0 μ M and 30.0 μ M.

Complex	3.0 μ M			30.0 μ M		
	WM well-matched	CC mismatched		WM well-matched	CC mismatched	
	max ei	max ei	max ei _{cc} / max ei _{WM}	max ei	max ei	max ei _{cc} / max ei _{WM}
1	941.0	2112.5	2.2	5584.5	11537.5	2.1
2	4640.0	4102.5	0.9	33233.0	47541.5	1.4
3	9896.5	10203.0	1.0	44345.5	47459.5	1.1
4	10412.5	11637.5	1.1	48816.0	64047.5	1.3
5	473.5	1188.0	2.5	3277.0	12877.0	3.9
6	1040.5	842.0	0.8	10017.0	8610.0	0.9

In accordance with the previous data, the signal for complex 4 with the methylated dppz functional group ligand displays the greatest emission intensity. Methylation of the bpy ancillary ligands lowers the intensity for complexes 2 and 3 although they are still brighter than complex 1.

Methylation of the bpy ancillary ligands in complexes 5 and 6, however, does not always reduce the signal below complex 1: for the well-matched 12mer, methylation at 4,4' raises it above complex 1 whilst methylation at 5,5' has the same effect for the CC mismatched 12mer at 30.0 μM .

Generally, larger differences in maximum emission intensity between the well-matched and CC mismatched 12mers were observed with $[\text{Ru complex}]:[\text{DNA}] = 10:1$ with the largest difference for complex 5. The increased signal for the CC mismatch is consistent with the results of the binding work with hairpin DNA (**Fig. 44**). This means that complex 5 with the unmethylated dppz functional group ligand and 5, 5' methylated bpy ancillary ligands seems to be the best photoprobe for the detection of the CC mismatch. The next most selective for the CC mismatch is complex 1 with complexes 2, 3 and 4 all showing some selectivity for the mismatch at a concentration of 30.0 μM . Fascinatingly, complex 6 gives a higher signal for the well-matched 12mer which means the difference in selectivity between methylation at the 5,5' and the 4,4' position on the ancillary ligand is more acute with this type of DNA (**Figs. 46 and 47**). Both complexes have the potential to identify the CC mismatch: the former via an increase in the signal and the latter through a reduction compared to well-matched DNA.

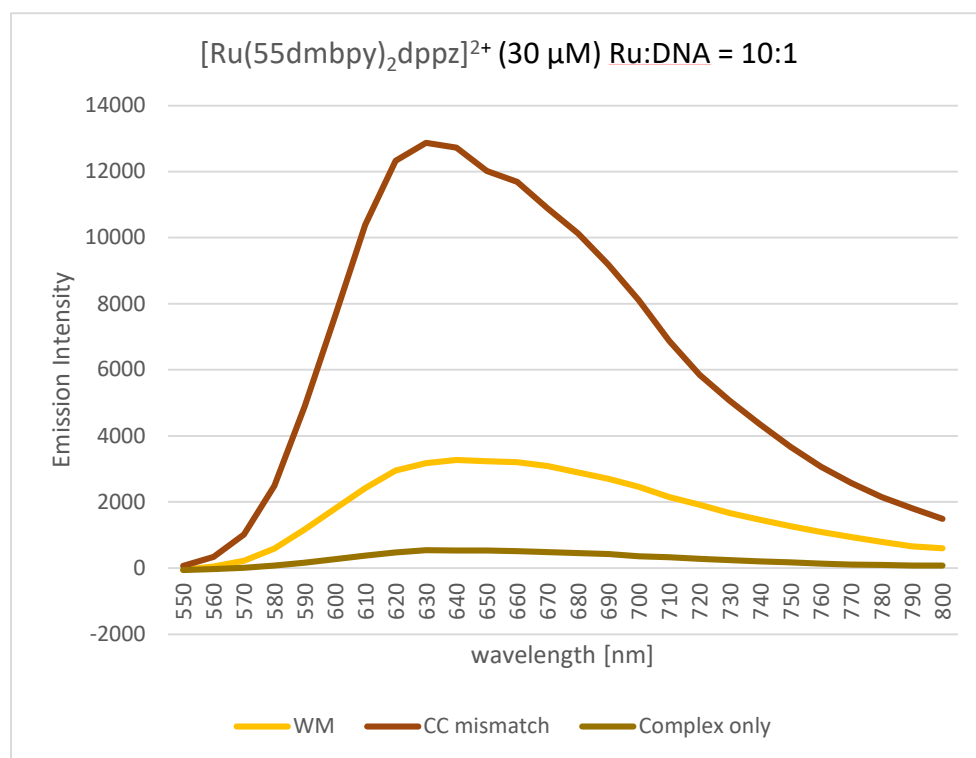


Fig. 46 Luminescence emission spectrum of complex 5 $[\text{Ru}(55\text{dmbpy})_2\text{dppz}]^{2+} = 30 \mu\text{M}$ in Tris buffer on addition of 12mers.

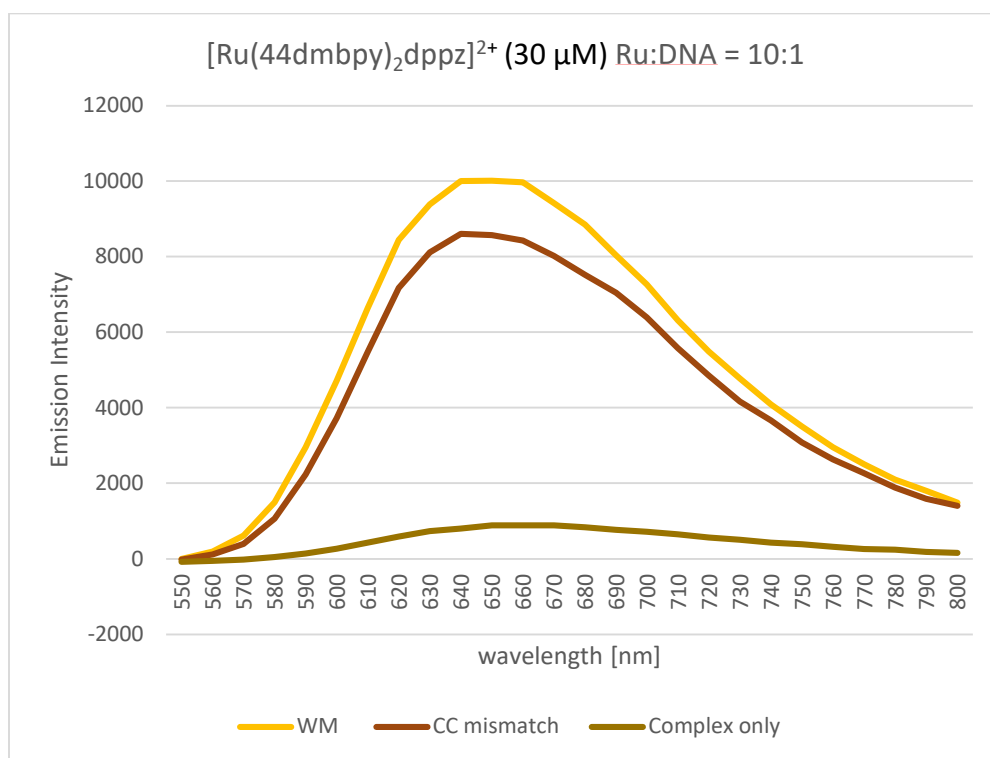


Fig. 47 Luminescence emission spectrum of complex 6 $[\text{Ru}(44\text{dmbpy})_2\text{dppz}]^{2+} = 30 \mu\text{M}$ in Tris buffer on addition of 12mers.

b) Luminescence via competitive displacement of ethidium bromide with complexes 1 to 8

Table 14. Apparent binding constants for complexes 1 to 8 in Tris buffer via EthBr displacement assay.

Complex	WM well-matched		CC mismatched		$K_{\text{app CC}}/K_{\text{app WM}}$
	Concentration of complex to reduce emission intensity by 50% C_{50}	Apparent binding constant $K_{\text{app WM}}$	Concentration of complex to reduce emission intensity by 50% C_{50}	Apparent binding constant $K_{\text{app CC}}$	
1	31.53	1.09E+06	27.93	1.23E+06	1.13
2	Not possible to calculate as luminescence did not reduce				
3					
4					
5	29.47	1.16E+06	22.88	1.50E+06	1.29
6*	30.18	1.14E+06	18.47	1.99E+06	1.74
7	18.81	1.82E+06	14.61	2.35E+06	1.29
8	17.95	1.91E+06	14.43	2.38E+06	1.25

* complex 6 was analysed using a new batch of 12mers and so its data were adjusted using the differences between the values for complex 1 with the new and original 12mers.

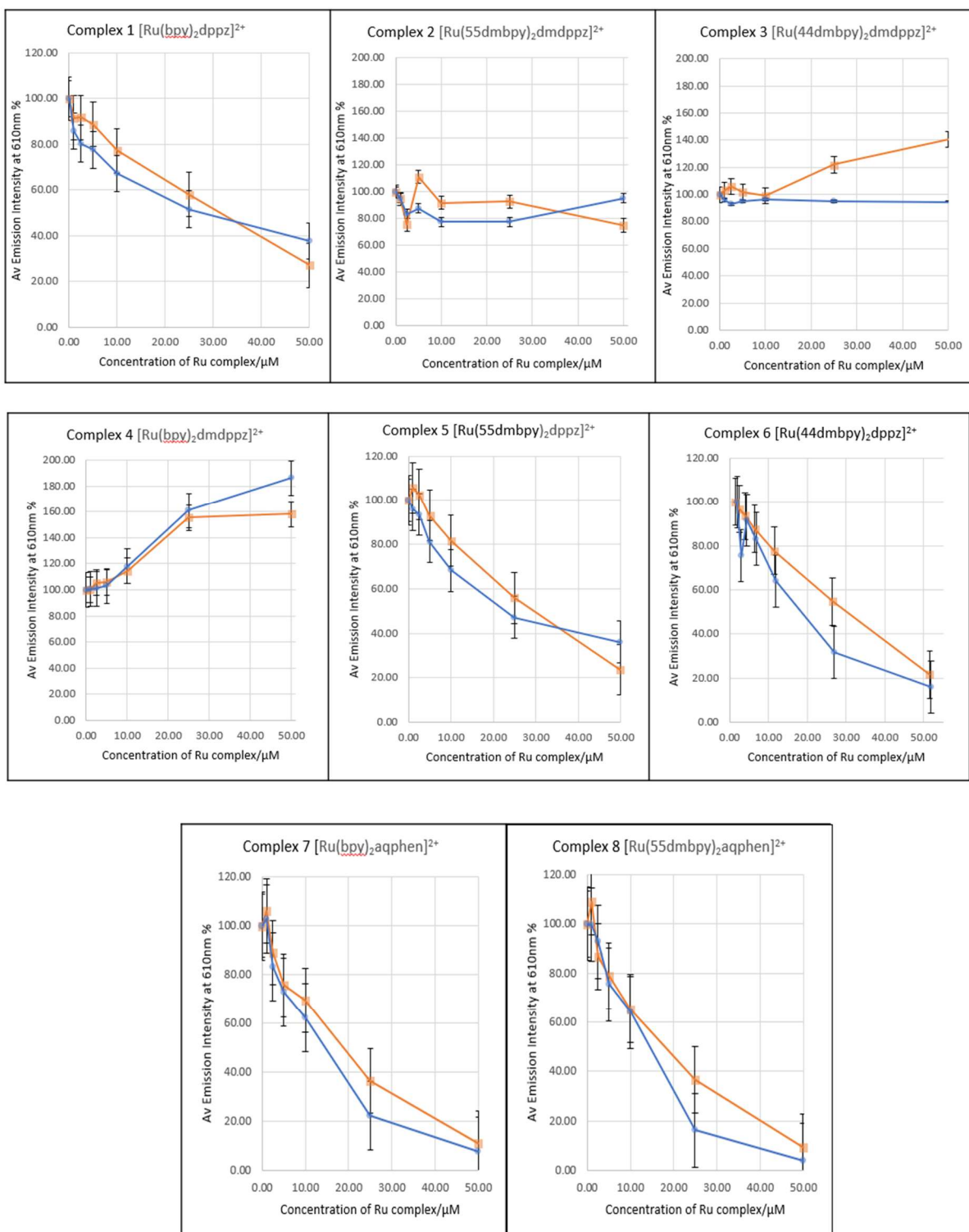


Fig. 48 EthBr displacement assays with 12mers: plots of average emission intensities at 610 nm vs [Ru complexes] in Tris buffer for complexes 1 to 8. Excitation wavelength = 530 nm.
 (a) ■ well-matched 12mer ● CC mismatched 12mer (b) 0.00 μM [Ru complex] = 100% emission intensity for all complexes.

EthBr is a fluorophore and classic DNA intercalator.⁴⁸ For complexes 2, 3 and 4 the fact that the luminescence did not decrease in the assay could mean that the EthBr is not being displaced (**Fig. 48**). This would, in turn, mean that these complexes, which all contain the 10,12 methylated dppz functional group ligand, are not binding to the DNA by intercalation. On the other hand it is possible that the EthBr is being displaced but the drop in signal is not observed due to the large increase in luminescence of the Ru complex when it intercalates into the DNA double helix. The Ru complexes show emission peaks from 600-623 nm and the EthBr emission is at 610nm. Also, even though the usual excitation wavelength for the Ru complexes is 450 nm, **Fig. 31** indicates a small absorption for complex 2 around 530 nm, which is the excitation wavelength for EthBr. For complexes 3 and 4 the absorption at 450 nm is broad and any smaller absorptions at 530 nm could have been subsumed within it.

Methylation of the ancillary bpy ligands in complexes 5 and 6 leads to stronger binding with the 12mers compared to complex 1 which does not have this steric bulk. This is in accordance with the CT DNA binding data although, as stated previously, the value for the binding constant for complex 6 with CT DNA could not be determined reliably because its data could not be fitted to the McGhee-von Hippel equation. The use of aqphen as the functional group ligand in complex 7 produces even greater apparent binding constants K_{app} with methylation of the ancillary bpy ligand in complex 8 resulting in further increases. This is again consistent with the calculation of binding affinities of complexes 7 and 8 with CT DNA using both UV/VIS and EthBr displacement methods.

The ratios of the apparent binding constants K_{app} for the CC mismatched and well-matched 12mers indicate that all these complexes bind with a greater affinity to the CC mismatched DNA compared to the well-matched sequence. This means they all have the potential to detect this least thermodynamically stable mismatch which could prove to be an exciting development if the mismatch can be linked to specific cancer causing mutations in MMR deficient cells. Methylation of the ancillary ligands increases the difference in binding for the dppz complexes with positions 4,4' causing a larger differential than positions 5,5'. The aqphen functional group ligand has a greater binding constant than dppz, although 5,5' ancillary group methylation in complex 8 does not appear to improve selectivity for the CC mismatch site.

As this work has focused on changes in binding constants and luminescence signals caused by methylation of the bpy ancillary and/or the dppz functional group ligands of the parent complex 1 $[Ru(bpy)_2dppz]^{2+}$. **Table 15** summarises all the changes by normalizing the data to the figures obtained for complex 1.

Table 15. Summary of binding affinity and luminescence data for complexes 1 to 8. All results normalised to complex 1 as the parent complex. K_b = binding constant. I_{max} = maximum luminescence intensity. K_{app} = apparent binding constant. WM = well-matched base pair. CC = CC mismatched base pair.

Complex	CT DNA				Hairpin DNA	12mer DNA			
	luminescence		UV/VIS	EthBr displace	luminescence	luminescence		EthBr displace	
	K_b	I_{max}	K_b	K_{app}	I_{max}	I_{max} WM	I_{max} CC	K_{app} WM	K_{app} CC
1	1.00	1.00	1.00	1.00	1.00	1.00	1.00	1.00	1.00
2	6.30	3.50			4.33	5.95	4.12		
3	3.60	4.40			3.77	7.94	4.11		
4	4.90	8.70			5.23	8.74	5.55		
5	1.20	0.40		1.07	0.89	0.59	1.12	1.06	1.22
6	1.80*	0.60			0.72	1.79	0.75	1.05	1.62
7			2.18	1.20				1.67	1.91
8			2.25	1.21				1.75	1.93

4. Conclusions

Methylation at positions 10 and 12 of the inserting dppz functional group ligand in complexes 2, 3 and 4 have resulted in large increases in emission intensity compared to the parent complex 1 $[\text{Ru}(\text{bpy})_2\text{dppz}]^{2+}$ with the three types of DNA studied: CT DNA, a 29mer hairpin and 12mer duplexes (**Table 15**). The signals for complexes containing this ligand could be explained by a combination of increased binding constants and larger quantum yields due to the addition of electron-donating methyl groups to the dppz ligand destabilizing the phenazine moiety (**Table 9**). However, the functionalization of the dppz by increasing steric bulk did not lead to notable differences in luminescence between mismatched and well-matched DNA and, in fact, decreased the inherent selectivity demonstrated by complex 1 $[\text{Ru}(\text{bpy})_2\text{dppz}]^{2+}$ (**Table 13**). This work could be further explored via the use of other electron-donating substituent groups such as -OH and -NH₂ as well as by having the methyl groups in positions 11 and 12 on the dppz ligand. Studies with methylation at position 10, position 11, positions 10 and 12 and positions 11 and 12 have focused on well-matched DNA only and so the interaction with mismatched DNA would be novel.⁵⁴

The suggestion that the methylated dppz ligand may not bind to DNA through intercalation could go some way towards explaining these findings. If, for example, the binding mode was metalloinsertion through the minor groove so that the ruthenium complex ends up deeply inserted into the helix then this would account for the large increase in signal. Another alternative to intercalation and metalloinsertion is groove binding but this would probably not draw the complex far enough into the helix to reduce the quenching by water to the extent observed. Metalloinsertion at mismatched base pair sites has been demonstrated alongside intercalation at well-matched sites and if both binding modes are in operation for complexes 2, 3 and 4 then this could account for the lack of selectivity.²⁶ However, it does not account for the lack of any reduction in luminescence in the competitive assay with EthBr. This could be explained if the methylated dppz ligand does bind through intercalation but the decrease in the EthBr signal at 610 nm is masked by the larger luminescence of complexes 2, 3 and 4 from 600-623 nm. Methylated dppz ligands have been shown to bind to well-matched DNA via intercalation albeit with different ancillary ligands.⁵⁴ The large emission intensities and strong binding affinities have been explained via the hydrophobic effect of the methyl groups in the DNA groove. Clearly steric factors and the angle of orientation of the complex are highly significant in determining the mode of binding and the luminescence and it is likely that complexes 2, 3 and 4 are intercalating into the DNA double-helix. However, the large signals could mean that differences between well-matched DNA and DNA with just one mismatched base pair are not observed.

Methylation of the ancillary bpy ligands lowers the luminescent signal of complexes 2 and 3 compared with complex 4 and for complexes 5 and 6 compared with complex 1. This is because the increased projection radii would hinder intercalation. 5,5' methylation results in lower luminescence than 4,4' methylation due to its larger ligand diameter and the data confirm this for the CT DNA and the well-matched 12mer DNA (**Table 15**). For the hairpin with CC and TT mismatched base pairs and the 12mer with a CC mismatch, the emission intensity is higher when the 5,5' positions on the ancillary bpy ligands are methylated compared to 4,4' methylation (**Figs. 42 and 43 and Table 15**). Compared to well-matched DNA, the signal for complex 5 is four times higher for the CC mismatch with the 12mer (**Table 13**) and more than six times higher for the same mismatch with the hairpin (**Fig. 44**); the latter compares very favorably with the six times increase quoted by Boynton *et al.* for the same complex.¹²

The data for the competitive displacement of EthBr from CT DNA and the 12mer duplexes suggest that intercalation is the binding mode when the ancillary bpy ligands are methylated for the dppz complexes 1, 5 and 6. The lower signals observed with methylation in this part of the complex (**Table 15**) are also consistent with intercalation in that the dppz functional group ligand is inserted between two adjacent base pairs but the complex does not end up completely embedded inside the helix as it would in the case of metalloinsertion.^{12,55} Nevertheless, the measured binding affinities do not account for the luminescence intensity observed as obviously as for the dppz functional group ligand. Methylation of the ancillary bpy ligands at the 5,5' or the 4,4' positions for complexes 5 and 6 results in very similar binding constants for the well-matched 12mer duplex but the latter has the higher signal. With the CC mismatched 12mer for the same complexes, 4,4' methylation has the larger K_{app} but 5,5' methylation the higher emission intensity (**Table 15**). This could be because the 12mer with the CC mismatch has eleven well-matched base pairs but just one mismatched pair. The binding constant is an average across all the sites and for complexes with 4,4' methylated ancillary bpy ligands K_{app} is likely to be higher because of its lower projection radius. So even though the complex with 5,5' methylated bpy ancillary ligands binds more strongly to the one CC mismatch, its average K_{app} is lower because of the excess of well-matched sites to which it binds less strongly than when the methyl groups are in the 4,4' positions.

This does not explain the similar binding affinities measured for the well-matched 12mer. The other possibility is that methylation at the 5,5' bpy positions gives rise to higher luminescence when the ruthenium complex is actually bound to the CC mismatched 12mer, even though it is not as strongly attracted to it beforehand as the complex with methylation at the 4,4' bpy positions. These data show that it cannot be assumed that emission intensity correlates directly with binding strength: it appears that stronger binding means a brighter signal when the dppz functional group ligand is methylated but methylation of the ancillary bpy ligands can result in a lower signal for a stronger binding affinity. This means that definite conclusions regarding binding constants for the dppz complexes 5 and 6 in relation to complex 1 cannot be drawn from this work. However, it can be inferred that the mode of binding is intercalation and that methylation of the ancillary bpy ligands in positions 5,5' in complex 5 produces a compound with a much higher luminescence for DNA with a CC or a TT mismatched base pair compared to DNA which is completely well-matched.

The introduction of the asymmetric, “elbow-shaped” aqphen ligand to complexes 7 and 8 as the inserting functional group ligand in place of dppz leads to a greater binding affinity with both CT DNA and the well-matched and CC mismatched 12mers. Methylation of the ancillary bpy ligands at the 5,5' positions results in minor increases in the binding constants which is consistent with the data for the same structural modification to $[\text{Ru}(\text{bpy})_2\text{dppz}]^{2+}$ with these three types of DNA (**Table 15**). The displacement assay with EthBr indicates that these complexes bind to DNA via intercalation of the inserting aqphen functional group ligand between adjacent base pairs. They are weakly emissive but the larger binding affinities compared to the dppz functional group implies greater intercalation into the helical structure of DNA.^{15,27} This could be due to increased hydrophobic interactions resulting from the extra aromatic ring and more hydrogen bonding with the quinone moiety. This would also explain why no mismatch selectivity difference was observed when substituting the bpy with 5,5' methylated bpy ancillary ligands as bonding and selectivity are dominated by the much larger aqphen ligand. That they have larger binding constants for the CC mismatched 12mers in comparison to the well-matched duplexes is an indication of potential selectivity for this least thermodynamically stable mismatch (**Table 14**). If this mismatch can be linked to specific mutations then this potential could be a significant development in the early detection and identification of related cancers. However, its therapeutic applications would need to be carefully investigated as intercalation does not remove the mismatched bases unlike metalloinsertion in which the CC or the TT pairing is extruded from the double-helix and replaced by an intercalating ligand (**Fig. 49**).

The aim of this work was to try to improve the selectivity of complex 1 for DNA mismatched base pairs through methylation of the ancillary bpy ligands, the dppz functional group ligand and then both simultaneously. This has been achieved through methylation of the ancillary bpy ligands in the 5,5' positions with dppz as the functional group ligand in complex 5. The difference in luminescence intensity for the CC mismatched relative to the well-matched DNA ranges from four to more than six times higher which represents a useful photoprobe for the identification of this mismatch, confirming the preliminary observations of Boynton *et al.* on the same complex.¹² This complex also has the potential to highlight a TT base pairing with a six fold increase for this mismatch in hairpin DNA which compares favourably to the work of Gill *et al.* for a bis $\text{Ru}(\text{dppz})$ complex and 10mer duplex.⁵⁶

Complexes 2, 3 and 4 with methylation at positions 10 and 12 on the dppz functional group ligand did have some selectivity for the CC and TT mismatches in hairpin DNA. However, the selectivity was reduced compared to methylation of the ancillary bpy ligands in the 5,5' positions for the unmethylated dppz complex. This appears to be the result of the overall brightness of signals from the methylated dppz complexes 2, 3 and 4 overriding any differences in luminescence resulting from the mismatches. The use of aqphen instead of dppz to enhance the steric bulk of the functional group ligand did improve selectivity in terms of the measurement of a greater binding affinity for the CC mismatch.

McConnell *et al.* suggested that future efforts to improve the mismatch specificity of $[\text{Ru}(\text{bpy})_2\text{dppz}]^{2+}$ should shift away from appending steric bulk to the distal portion of the dppz ligand.²⁷ This was because the structural modifications they had employed to increase the steric bulk of the dppz framework were not sufficient by themselves to enhance the luminescence differential between well-matched and mismatched DNA; the use of aqphen as a replacement for dppz is in keeping with this proposal.

Future work

Complex 5 proved to be the best photoprobe of the eight complexes synthesized for the identification of CC and TT mismatched DNA base pairs. As explained, if these mismatches can be linked to certain mutations which could be the starting points for cancers then this means it has real potential as an early warning, diagnostic tool. The next steps would be to test complex 5 with oligonucleotide duplex DNA containing a CC and then a TT mismatch which is shorter and as well as one which is longer than 12 base pairs. Further mismatches should also be investigated.

Although it is most likely that the mode of binding is intercalation, this need to be checked. This study has employed all the complexes as racemic mixtures. The use of a chiral selector during synthesis would enable resolution of the Δ and Λ enantiomers which would, in turn, mean that crystals of DNA containing the separate enantiomers of complex 5 could be prepared. Often such crystals will have different binding affinities and geometries which can be investigated via X-ray crystallography and the use of software such as UCSF Chimera to visualize the structures.^{57,58} It would show the precise mechanism by which the complexes interact with the DNA and confirm intercalation or metalloinsertion (**Fig. 49**) as well as providing some insight into why 5,5' methylation of the ancillary bpy ligands causes such a large signal increase with CC and TT mismatches.¹² However, it is also important to note that the interactions in a solid crystal could be different to those taking place in aqueous solution and *in vivo*.

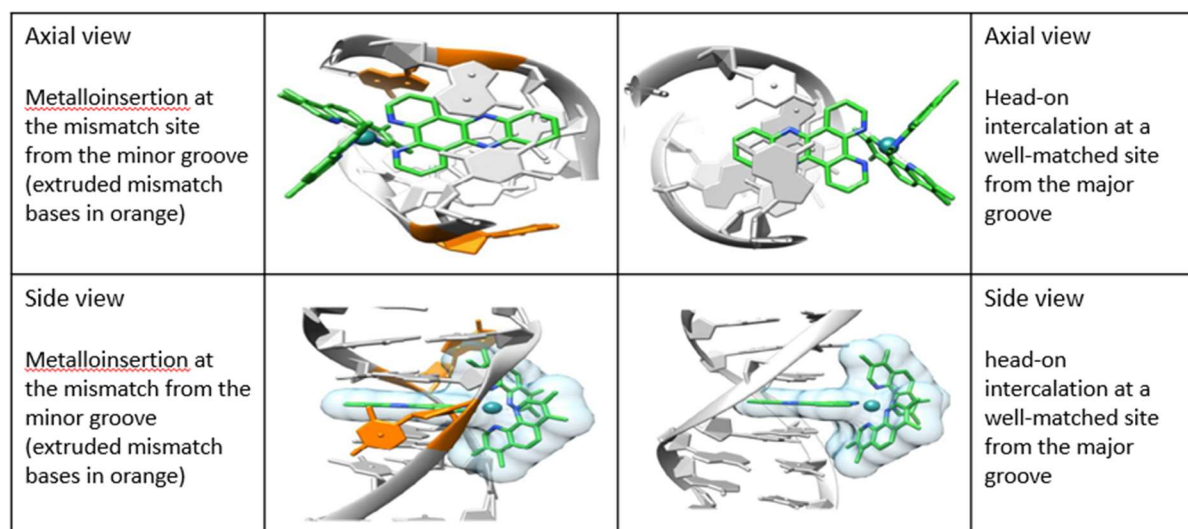


Fig. 49¹² Δ -[Ru(Me₄phen)₂dppz]²⁺ modelled into the crystal structures of DNA duplexes. Optimisation and visualization carried out using UCSF Chimera.⁵⁸

Other experiments which could be conducted to provide evidence for an intercalative binding mode include thermal denaturation and viscosity studies.^{36,59} The former through the intercalation of small molecules into the double helix of the DNA which would increase the temperature at which it melts to form single strands. The latter works via Ru complexes added to the DNA intercalating into the base stack, unwinding and elongating it, thus raising its viscosity. Metalloinsertion tends to take place through the minor groove and this could, in turn, be investigated by adding a minor groove quencher such as $[\text{Cu}(\text{phen})_2]^{2+}$ which would displace the Ru complex and reduce the luminescence.^{9,25}

The next stage for complex 5 would be to look at its cellular uptake followed by its ability to target the nucleus and, therefore, interact with DNA in live cells. Confocal Laser Scanning Microscopy (CLSM) can be used for this purpose.³⁶ Even if the uptake into live cells is limited the complex could still be useful as a nuclear imaging agent in fixed permeabilised cells. Looking even further forward, as mentioned, intercalation into the DNA base stack means that complex 5 does not remove any mismatched base pairs and so its cytotoxicity would need to be investigated. This could be done via a Thiazolyl Blue Tetrazolium Bromide (MTT) assay in which the concentration of complex 5 required to induce 50 % cell viability (IC_{50}) could be measured and compared with other chemotherapy drugs such as cisplatin or mitoxantrone.^{14,36,60}

References

- 1 F. I. Lu, C. B. Gilks, A. M. Mulligan, P. Ryan, G. Allo, K. Sy, P. A. Shaw, A. Pollett and B. A. Clarke, *Int. J. Gynecol. Pathol.*, 2012, **31**, 524–531.
- 2 N. Watson, F. Griefu, M. Morris, J. Harvey, C. Stewart, L. Schofield, J. Goldblatt and B. Lacopetta, *J. Mol. Diagn.*, 2007, **9**, 472–478.
- 3 A. Granzhan, N. Kotera and M.-P. Teulade-Fichou, *Chem. Soc. Rev.*, 2014, **43**, 3630.
- 4 Q. Deraedt, L. Marcélis, F. Loiseau and B. Elias, *Inorg. Chem. Front.*, 2017, **4**, 91.
- 5 F. Pierard and A. Kirsch-De Mesmaeker, *Inorg. Chem. Commun.*, 2006, **9**, 111–126.
- 6 B. M. Zeglis, V. Erie, C. Pierre, J. T. Kaiser and J. K. Barton, *Biochemistry*, 2009, **48**, 43.
- 7 A. Nano, J. Dai, J. M. Bailis and J. K. Barton, *Biochemistry*, 2021, **60**, 2055–2063.
- 8 K. M. Boyle and J. K. Barton, *J. Am. Chem. Soc.*, 2018, **140**, 5612–5624.
- 9 A. N. Boynton, L. Marcélis, A. J. McConnell and J. K. Barton, *Inorg. Chem.*, 2017, **56**, 8381–8389.
- 10 Q. Deraedt, L. Marcélis, T. Auvray, G. S. Hanan, F. Loiseau and B. Elias, *Eur. J. Inorg. Chem.*, 2016, **2016**, 3649–3658.
- 11 E. Ruba, J. R. Hart and J. K. Barton, *Inorg. Chem.*, 2004, **43**, 4570–4578.
- 12 A. N. Boynton, L. Marcélis and J. K. Barton, *J. Am. Chem. Soc.*, 2016, **138**, 5020–5023.
- 13 Y. Sun, D. A. Lutterman and C. Turro, *Inorg. Chem.*, 2008, **47**, 6427–6434.
- 14 M. R. Gill and J. A. Thomas, *Chem. Soc. Rev.*, 2012, **41**, 3179–3192.
- 15 B. M. Zeglis, V. C. Pierre and J. K. Barton, *Chem. Commun.*, 2007, **44**, 4565–4579.

- 16 G. Li, L. Sun, L. Ji and H. Chao, *Dalton Trans.*, 2016, **45**, 13265.
- 17 J. R. Lakowicz, *Principles of Fluorescence Spectroscopy*, Springer, 2006.
- 18 G.G. Stokes, *Phil. Trans. R. Soc. (London)*, 1852, **142**, 463–562.
- 19 M. Kasha, *Discuss. Faraday Soc.*, 1950, **9**, 14–19.
- 20 A. E. Friedman, J.-C. Chambron, J.-P. Sauvage, N. J. Turro and J. K. Barton, *J. Am. Chem. Soc.*, 1990, **112**, 4960–4962.
- 21 E. J. C. Olson, D. Hu, A. Ho, A. M. Jonkman, M. R. Arkin, E. D. A. Stemp, J. K. Barton and P. F. Barbara, *J. Am. Chem. Soc.*, 1997, **119**, 11458–11467.
- 22 A. W. McKinley, P. Lincoln and E. M. Tuite, *Coord. Chem. Rev.*, 2011, **255**, 2676–2692.
- 23 M. K. Brennaman, T. J. Meyer and J. M. Papanikolas, *J. Phys. Chem.*, 2004, **108**, 9938–9944.
- 24 R. M. Hartshorn and J. K. Barton, *J. Am. Chem. Soc.*, 1992, **114**, 5919–5925.
- 25 M. H. Lim, H. Song, E. D. Olmon, E. E. Dervan and J. K. Barton, *Inorg. Chem.*, 2009, **48**, 5392–5397.
- 26 H. Song, J. T. Kaiser and J. K. Barton, *Nat. Chem.*, 2012, **4**, 615–620.
- 27 A. J. McConnell, M. H. Lim, E. D. Olmon, H. Song, E. E. Dervan and J. K. Barton, *Inorg. Chem.*, 2012, **51**, 12511–12520.
- 28 S. Bodige and F. M. MacDonnell, *Tetrahedron Lett.*, 1997, **38**, 8159–8160.
- 29 J. Bolger, A. Gourdon, E. Ishow and J.-P. Launay, *Inorg. Chem.*, 1996, **35**, 2937–2944.
- 30 Giordano P, Randolph Bock C and Wrighton M, *J. Am. Chem. Soc.*, 1978, **100**, 6960–6965.
- 31 R. A. Smith, E. C. Stokes, E. E. Langdon-Jones, J. A. Platts, B. M. Kariuki, A. J. Hallett and S. J. A. Pope, *Dalton Trans.*, 2013, **42**, 10351.
- 32 B. Brandner, Implementation of a comparative method for measuring photoluminescence quantum yield of novel compounds in solution, <https://ir.library.oregonstate.edu/downloads/p2676w829>, (accessed October 25, 2021).
- 33 A. M. Brouwer, *Pure Appl. Chem.*, 2011, **83**, 2223.
- 34 Annealing Oligonucleotides Protocol, <https://www.sigmaaldrich.com/GB/en/technical-documents/protocol/genomics/pcr/annealing-oligos>, (accessed March 9, 2022).
- 35 Y. Zhang, G. Zhang, Y. Li and Y. Hu, *J. Agric. Food Chem.*, 2013, 2639.
- 36 M. R. Gill, H. Derrat, C. G. W. Smythe, G. Battaglia and J. A. Thomas, *ChemBioChem*, 2011, **12**, 877–880.
- 37 V. G. Vaidyanathan and B. U. Nair, *J. Inorg. Biochem.*, 2002, **91**, 405–412.
- 38 J. Feher, *Quantitative Human Physiology An Introduction*, Elsevier, 2017, 853–869.

- 39 SigmaPlot - Scientific Data Analysis and Graphing Software,
<http://www.sigmaplot.co.uk/products/sigmaplot/sigmaplot-details.php>, (accessed March 9, 2022).
- 40 J. D. McGhee and P. H. von Hippel, *J. Mol. Biol.*, 1974, **86**, 469–489.
- 41 L. M. Chen, J. Liu, J. C. Chen, C. P. Tan, S. Shi, K. C. Zheng and L. N. Ji, *J. Inorg. Biochem.*, 2008, **102**, 330–341.
- 42 C. Metcalfe, I. Haq and J. A. Thomas, *Inorg. Chem.*, 2004, **43**, 318–319.
- 43 M. McCann, J. McGinley, K. Ni, M. O’Connor, K. Kavanagh, V. McKee, J. Colleran, M. Devereux, N. Gathergood, N. Barron, A. Prisecaru and A. Kellett, *Chem. Commun.*, 2013, **49**, 2341–2343.
- 44 Calculation of molecular properties and bioactivity score,
<https://molinspiration.com/cgi-bin/properties>, (accessed December 13, 2021).
- 45 J. Olofsson, L. M. Wilhelmsson and P. Lincoln, *J. Am. Chem. Soc.*, 2004, **126**, 15458–15465.
- 46 G. D. Hager3 and G. A. Crosby, *J. Am. Chem. Soc.*, 1975, **97**, 7031–7037.
- 47 A. B. Pradhan, L. Haque, S. Bhuiya and S. Das, *RSC Adv.*, 2014, **4**, 52815–52824.
- 48 N. C. Garbett, N. B. Hammond and D. E. Graves, *Biophys. J.*, 2004, **87**, 3974–3981.
- 49 L.-M. Tumir, M. R. Stojković and I. Piantanida, *Beilstein J. Org. Chem.*, 2014, **10**, 2930–2954.
- 50 Marvin | ChemAxon,
<https://chemaxon.com/products/marvin>, (accessed December 5, 2021).
- 51 H. Xu, K. C. Zheng, H. Deng, L. J. Lin, Q. L. Zhang and L. N. Ji, *New J. Chem.*, 2003, **27**, 1255–1263.
- 52 Origin: Data Analysis and Graphing Software,
<https://www.originlab.com/index.aspx?go=PRODUCTS/Origin>, (accessed March 12, 2022).
- 53 B. A. Jackson and J. K. Barton, *Biochemistry*, 2000, **39**, 6176–6182.
- 54 J. P. Hall, H. Beer, K. Buchner, D. J. Cardin and C. J. Cardin, *Organometallics*, 2015, **34**, 2481–2486.
- 55 A. N. Boynton, *Targeting DNA Mismatches with Luminescent Ruthenium Complexes Thesis*, 2017.
- 56 M. R. Gill, M. G. Walker, S. Able, O. Tietz, A. Lakshminarayanan, R. Anderson, R. Chalk, A. H. El-Sagheer, T. Brown, J. A. Thomas and K. A. Vallis, *Chem. Sci.*, 2020, **11**, 8936–8944.
- 57 I. Haq, P. Lincoln, D. Suh, B. Norden, B. Z. Chowdhry and J. B. Chaires, *J. Am. Chem. Soc.*, 1995, **117**, 4788–4796.
- 58 UCSF Chimera Home Page,
<https://www.cgl.ucsf.edu/chimera/>, (accessed March 14, 2022).
- 59 P. v Scaria and R. H. Shafer, *J. Biol. Chem.*, 1991, **266**, 5417–5423.
- 60 Z. Jendželovská, R. Jendželovský, L. Hilovská, J. Koval, J. Mikeš and P. Fedoročko, *Toxicol. In Vitro*, 2014, **28**, 1259–1273.